

1 Context-dependent functional compensation between Ythdf m⁶A 2 readers

3
4 Lior Lasman¹, Vladislav Krupalnik¹, Shay Geula², Mirie Zerbib¹, Sergey Viukov¹, Nofar Mor¹, Alejandro
5 Aguilera Castrejon¹, Orel Mizrahi¹, Sathe Shashank³, Aharon Nachshon¹, Dan Schneir¹, Stefan Aigner³,
6 Archana Shankar³, Jasmine Mueller³, Noam Stern-Ginossar¹, Gene W Yeo³, Noa Novershtern¹@, Jacob H
7 Hanna¹@

8 ¹ The Department of Molecular Genetics, Weizmann Institute of Science, Rehovot 7610001, Israel.

9 ² Children's Research Institute, UT Southwestern Medical Center, Dallas, TX 75235

10 ³ The Department of Cellular and Molecular Medicine, University of California, San Diego, La Jolla, CA 92093.

11 @ Correspondence should be addressed to Noa Novershtern (noa.novershtern@weizmann.ac.il) and Jacob H. Hanna
12 (jacob.hanna@weizmann.ac.il)

13

14 Abstract

15

16 The N6-methyladenosine (m⁶A) modification is the most prevalent post-transcriptional mRNA
17 modification, regulating mRNA decay, translation and splicing. It plays a major role during normal
18 development, differentiation, and disease progression. The modification is dynamically regulated
19 by a set of writer, eraser and reader proteins. The YTH-domain family of proteins: Ythdf1, Ythdf2,
20 and Ythdf3, are three homologous m⁶A binding proteins, which have different cellular functions.
21 However, their sequence similarity and their tendency to bind the same targets suggest that they
22 may have overlapping roles. We systematically knocked out (KO) the Mettl3 writer for each of
23 the Ythdf readers and for the three readers together (triple-KO). We then estimated the effect
24 *in-vivo*, in mouse gametogenesis and viability, and *in-vitro*, in mouse embryonic stem cells
25 (mESCs). We show that in gametogenesis, Mettl3-KO severity is increased as the deletion occurs
26 earlier in the process, and Ythdf2 has a dominant role that cannot be compensated by Ythdf1 or
27 Ythdf3, possibly due to differences in readers' expression, both in quantity and in spatial location.
28 By knocking out the three readers together and systematically testing offspring genotypes, we
29 have revealed a redundancy in the readers' role during early development, a redundancy which
30 is dosage-dependent. Additionally, we show that in mESCs there is compensation between the
31 three readers, since the inability to differentiate and the significant effect on mRNA decay occur
32 only in the triple-KO cells and not in the single KOs. Thus, we suggest a novel model for the Ythdf
33 readers function. There is a dosage-dependent redundancy when all three readers are co-
34 expressed in the same location in the cells.

35

36 Introduction

37

38 RNA modifications are a layer of gene expression regulation, similar to DNA and protein
39 modifications (Heck and Wilusz 2019). N6-methyladenosine, also known as m⁶A, is the most
40 abundant mRNA modification (Heck and Wilusz 2019). It was first discovered in the 70's, but
41 major progress was done in recent years due to new approaches of mapping m⁶A sites
42 (Dominissini et al. 2012; Meyer et al. 2012; Garcia-Campos et al. 2019). Its importance was shown

43 in a wide range of organisms and processes, from yeast meiosis (Schwartz et al. 2013), sex
44 determination in drosophila (Kan et al. 2017), and up to mammalian early development (Geula
45 et al. 2015), neural development (Wang et al. 2018) and hematopoiesis (Lee et al. 2019).

46
47 m⁶A modification is highly regulated by writer, reader and eraser proteins. Mettl3 forms a
48 heterodimer with Mettl14 (Liu et al. 2014), and together with the supporting WTAP protein,
49 catalyzes m⁶A with preference to 3'UTR, 5'UTR, long exons, and near stop codons (Heck and
50 Wilusz 2019). FTO and Alkbh5 are eraser enzymes found in vertebrates (Zheng et al. 2013; Jia et
51 al. 2011), and potentially have distinct role and localization in the cell (Zheng et al. 2013; Wei et
52 al. 2018).

53
54 Multiple proteins were identified as m⁶A readers, with the YTH domain-containing proteins
55 (Ythdf and Ythdc) stand out among them. Recent studies link these proteins to different functions
56 in RNA metabolism: Ythdf1 and Ythdf3 were shown to promote translation by recruiting
57 translation initiation factors in HeLa cells (Shi et al. 2017; Wang et al. 2015; Li et al. 2017), Ythdf2
58 was linked to degradation, partially by recruiting the CCR4-NOT deadenylase complex (Du et al.
59 2016; Wang et al. 2014), and nuclear Ythdc1 was shown to regulate splicing (Kasowitz et al. 2018;
60 Hartmann et al. 1999). Ythdf1, 2 & 3 share high protein sequence similarity (67-70%, **Figure S1a**).
61 In addition, they have co-evolved during evolution. While *Drosophila melanogaster* has one copy
62 of Ythdf protein (named Ythdf), vertebrates have three functional proteins (**Figure S1b**), probably
63 generated following duplication events (Pervaiz et al. 2019).

64
65 It is not fully clear whether each one of the Ythdf readers fulfills a distinct role. Their sequence
66 similarity, and that they are all localized in the cytoplasm (Wang et al. 2015, 2014; Shi et al. 2017)
67 and share many of their targets (Li et al. 2017; Patil et al. 2016, 2018) indicate partial redundancy.
68 However, knockout (KO) of Ythdf2 alone is sufficient to stop proper oocyte maturation (Ivanova
69 et al. 2017), and a single KO of Ythdf1 or of Ythdf2 causes neural defects (Li et al. 2018; Shi et al.
70 2018), suggesting that in certain systems, Ythdf readers cannot compensate each other. This
71 however could be a result of differences in expression levels in the different tissues.
72 Comprehensive research into the redundancy between the three Ythdfs has not been conducted.
73 In addition, the effect of knocking out the three readers *in-vivo* has not been described so far.

74
75 In this study we use conditional single KOs of Mettl3 and Ythdf1, 2 & 3, and show that both Mettl3
76 and Ythdf2 are essential for proper gametogenesis, and that mice lacking these proteins are
77 either hypo-fertile or sterile. The severity of the phenotype is increased when the Mettl3 deletion
78 is done earlier in the process. We found that the Ythdf readers have different expression patterns
79 during gametogenesis, which might explain the lack of compensation in this process. In addition,
80 we generated an *in vivo* triple-KO and found that it leads to impaired development as early as

81 E7.5, and to embryonic lethality. By using systematic genotyping of viable offspring, we found
82 that in early development there is compensation between the readers, which is dosage-
83 dependent, i.e. Ythdf2-heterozygous mice need to have at least one functional copy of another
84 Ythdf reader to escape mortality. Furthermore, we used mESCs to analyze the function of each
85 Ythdf reader separately, and together. We found that only triple-KO mESCs are not able to
86 differentiate properly, and present a prolonged mRNA degradation rate, similar to the effect
87 shown in Mettl3-KO, while no significant effect is seen in the single-KOs. This suggests that just
88 like in early development, in mouse ESCs, a system in which all the readers are expressed in the
89 same cells and compartment, there is a redundancy between Ythdf readers, which enables
90 compensation in the absence of the other.

91

92 **Results**

93

94 **Mettl3 writer plays an essential role in oogenesis and spermatogenesis**

95

96 We started by systematically testing the three readers in a specific system *in-vivo*, focusing on
97 spermatogenesis and oogenesis. m⁶A writers Mettl3 and Mettl14 and m⁶A erasers FTO and
98 ALKBH5 were found to be essential for proper gametogenesis in mouse. Their KO typically leads
99 to defective maturation of sperm or ova, and hypofertility (Xu et al. 2017; Lin et al. 2017; Zheng
100 et al. 2013; Tang et al. 2017; Lasman, L, Hanna, JH, Novershtern 2020; Kasowitz et al. 2018).

101 As for m⁶A readers, both Ythdc1 and Ythdc2 have an essential role in gametogenesis. Their KO in
102 spermatogenesis or oogenesis leads to a severe hypofertility phenotype (Hsu et al. 2017; Bailey
103 et al. 2017; Wojtas et al. 2017; Jain et al. 2018; Kasowitz et al. 2018). Knocking out Ythdf2 leads
104 to normal ovulation but an inability to downregulate maternal mRNA. Thus, Ythdf2-KO females
105 are sterile (Ivanova et al. 2017). In contrast, Ythdf2-KO males show normal seminiferous tubule
106 histology (Ivanova et al. 2017). Depletion of Ythdf2 in mouse spermatogonia leads to defective
107 cell morphology and decreases cell proliferation (Huang et al. 2020). However, further
108 examination of all Ythdf readers in spermatogenesis is still required.

109

110 We assessed the importance of m⁶A in gametogenesis, both in males and females, using
111 conditional KOs of the m⁶A writer Mettl3 (**Figure S2**). Mettl3^{flox/flox} mice were crossed with mice
112 carrying one of the following Cre constructs: ZP3-Cre which is activated during oogenesis, Stra8-
113 Cre and Prm1-Cre, which are activated during spermatogenesis, and Vasa-Cre which is activated
114 in the early stages of both. Thus, we could test the effect of Mettl3-KO systematically in different
115 time points during gametogenesis, in both males and females.

116

117

118 Mettl3^{f/f}Vasa-cre+ KO had a major effect on oocyte development. A dissection of Mettl3^{f/f}Vasa-
119 cre+ female mice showed abnormal ovary morphology (**Figure 1a-b**), and the mice were sterile
120 (**Figure 1c**). Zp3 is expressed during a later stage of the oocyte maturation, prior to the
121 completion of the first meiosis (Gao et al. 2017a). Accordingly, Mettl3^{f/f}Zp3-cre+ female mice
122 showed a normal ovary morphology (**Figure 1d**). However, the mice were sterile (**Figure 1e**).
123 Flushing oocytes from the oviduct revealed an overall significant low number of oocytes (p-value
124 <0.002, **Figure 1f**). All the flushed oocytes of the KO were stuck at the germinal vesicle (GV) stage
125 and did not reach the two-cell stage upon fertilization attempts (**Figure 1g, S3a**), meaning that
126 they have not completed the first meiosis. Indeed, immunostaining of tubulin in KO and WT
127 oocytes, showed that KO oocytes were stuck in the GV stage, and did not proceed for GV
128 breakdown and completion of the first meiosis (**Figure 1h**). The transcriptional profile of Mettl3-
129 cKO and control oocytes revealed a major change in transcription (**Figure S3b**), including aberrant
130 expression of genes related to oocyte development (**Figure S3c-d, Table S1**).
131

132 Next, we tested the role of Mettl3 in spermatogenesis. Mettl3^{f/f}Vasa-cre+ male mice, in which
133 the KO was activated during primordial germ cells, showed a massive reduction in the testis
134 volume (**Figure 2a**), severe degenerative defects (**Figure S4a**), and sterility (**Figure 2b**), as was
135 reported elsewhere (Xu et al. 2017; Lin et al. 2017). Similarly, a dissection of Mettl3^{f/f}Stra8-cre+
136 male mice, in which the KO was activated during early-stage spermatogonia, showed a
137 significantly reduced testis volume (**Figure 2c**), mild degenerative changes in seminiferous
138 tubules (**Figure S4b**), and ~75% reduction in sperm quantity observed in the cauda epididymis
139 (**Figure S4b**). Indeed, Mettl3^{f/f}Stra8-cre+ mice showed significant hypofertility compared to their
140 counterpart control (**Figure 2d**), similar to what was previously reported (Lin et al. 2017).
141 Interestingly, Mettl3^{f/f}Prm1-cre+ male mice, in which the KO was activated in the spermatids
142 (**Figure 2e**), showed normal fertility (**Figure 2f**) and typical seminiferous tubules morphology
143 (**Figure S4c**).
144

145 In summary, our genetic dissection of Mettl3's role during gametogenesis shows the pivotal role
146 of m⁶A modifications in both oogenesis and spermatogenesis. The severity of the phenotype was
147 dependent on the stage in which Mettl3 was depleted. Therefore, we tested the effect of Ythdf
148 KO, which might have a milder effect on the process.

149
150 **Ythdf2 is the only Ythdf reader which is essential for gametogenesis, and has a different**
151 **expression pattern than Ythdf1 and Ythdf3**

152
153 To understand the role of the Ythdf family in gametogenesis, we knocked out each of the three
154 readers using CRISPR-Cas9 (**Figure S1c**). Heterozygous mice were further crossed to give full KO
155 for each of the Ythdfs. The mice that were born were validated by genotyping (**Figure S1d**).

156 Ythdf1^{-/-} and Ythdf3^{-/-} mice were born in the expected Mendelian ratio (**Figure 3a**) and showed
157 no apparent defects. However, 80-83% of Ythdf2^{-/-} pups died shortly after birth, leading to a sub-
158 Mendelian ratio 30 days after birth (**Figures 3a**).

159 Ythdf1-KO and Ythdf3-KO mice were fertile as their control counterparts (**Figure S5a-d**) and did
160 not show any histological defect in their reproductive organs (**Figure S5e-f**). As for Ythdf2, the
161 few viable KO mice that survived were tested. While Ythdf2-KO female mice showed normal
162 oocyte morphology (**Figure S6a**), they were sterile (**Figure S6b**), suggesting a later defect than
163 what was observed in Mettl3^{f/f}Zp3-cre⁺ oocytes. Indeed, a recent work showed that Ythdf2-KO
164 oocytes could be fertilized but do not develop beyond the 8-cell stage, probably because of their
165 inability to reduce maternal RNA (Ivanova et al. 2017). Next, the oocytes were flushed after
166 hormone priming and measured for RNA levels using SMART-seq. Although the morphology was
167 indistinguishable from WT, on the molecular level, the cells of Ythdf2-KO were already distinctly
168 clustered compared to WT (**Figure S6c**). Among the 311 genes that were downregulated in the
169 KO (**Table S1**), 72 are related to extracellular matrix (p<1.35e-06), which is crucial for oocyte
170 fertility. Interestingly, in sperm too, m⁶A regulation of metallopeptidase is mediated by Ythdf2
171 (Huang et al. 2020).

172 Ythdf2-KO male mice showed mild degenerative changes in the seminiferous tubules (**Figure**
173 **S4d**), and severe loss of sperm in the cauda epididymis (**Figure S4e**). Accordingly, these males
174 were hypofertile (**Figure 2g**). Measuring expression in WT and KO round sperm cells, we observed
175 changes in expression in 301 genes (**Figure S4f, Table S1**), many of them associated with
176 cytoskeleton, microtubules and cilium functions (**Figure S4f**), possibly explaining the impaired
177 sperm maturation. In addition, some metallopeptidases were up-regulated in the KO (e.g.
178 Adam4, Adamts3, Cpxm1).

179
180 Although Ythdf1 and Ythdf3 share high sequence homology with Ythdf2, they cannot compensate
181 for its depletion during gametogenesis. One possible explanation for this observation is that the
182 proteins are not expressed in the same spatial or temporal space during the process. To test this
183 hypothesis, we immunostained histological sections of the testis for different reader expression.
184 Indeed, immunostaining of seminiferous tubules showed that Ythdf1, Ythdf2 and Ythdf3 are
185 expressed in different cells during the sperm maturation process (**Figure 2h**). Similarly, staining
186 of GV oocytes showed a different expression pattern for Ythdf2, as it is the only Ythdf reader that
187 is located both in the cytoplasm and nucleus (**Figures 1i, S7**). Thus, the different expression
188 pattern of the Ythdf readers in gametogenesis may explain the lack of compensation for Ythdf2
189 depletion.

190
191 **Ythdf readers compensate one another in a dosage-dependent manner in early development**

192

193 Next, we tried to generate Ythdf triple-KO mice for a more comprehensive understanding of the
194 readers' roles *in-vivo*. Ythdf1^{-/-} and Ythdf3^{-/-} mice were crossed, and the double heterozygote
195 offspring were further crossed with Ythdf2^{+/-} mice to generate triple heterozygote mice to all
196 three readers (Ythdf1^{+/-}Ythdf2^{+/-}Ythdf3^{+/-} or "triple-HET") (**Figure 3b**). Triple-HET mice were
197 crossed, and all their offspring (n=200) were genotyped on day 30 post-natal (**Figure 3c**). The
198 ratio of offspring with Ythdf2-WT genotype was as or above the expected Mendelian-ratio, while
199 no offspring with Ythdf2-KO were detected. Interestingly, even when the mice were only
200 heterozygote for Ythdf2 (Ythdf2^{+/-}), the Mendelian-ratio of offspring with another missing reader
201 was below the expected ratio (Ythdf1^{-/-}2^{+/-}3^{+/-}, threefold below expected, Ythdf1^{+/-}2^{+/-}3^{-/-},
202 fourfold below expected, p<0.012). Moreover, we could not detect any offspring which were
203 Ythdf2^{+/-} and null in the two other readers (Ythdf1^{-/-}Ythdf2^{+/-}Ythdf3^{-/-}). These results suggest that
204 lack of Ythdf1 or Ythdf3 can be compensated by the two other readers. However, the lack of
205 Ythdf2 cannot be compensated by Ythdf1 or Ythdf3. In addition, the fact that partial expression
206 of Ythdf2 in the heterozygous lineage requires the expression of at least one other reader,
207 suggests that the function of the readers is dosage-dependent, and that a certain threshold of
208 Ythdf readers are needed to be expressed in the cell to accomplish their function.

209

210 To better understand in which stage of development the triple-KO is defected, we analyzed triple-
211 KO embryos on embryonic day 7.5 (E7.5). We found that already in this early stage of the post-
212 implantation development, the triple-KO embryos were broadly deformed compared to the WT
213 control (**Figure 3d**).

214

215 **Triple-KO mESCs show normal self-renewal ability, but have an impaired ability to** 216 **differentiate**

217

218 We found that the Ythdf proteins can compensate one another *in-vivo* when expressed in the
219 same cells, and that this compensation is dosage-dependent. Next, we wanted to better
220 understand the molecular mechanism in which the different Ythdfs process mRNA molecules and
221 thus affect cell viability and differentiation potential. We hypothesized that mESCs would be a
222 good model for studying the molecular role of the readers *in-vitro*, since this is a system in which
223 we can systematically perturb the cells and test the stem-cell activity outcomes (self-renewal and
224 differentiation). In addition, in contrast to gametogenesis, all of the Ythdf readers are expressed
225 in the same cells (**Figure 4a**) thus enabling us to test different compensation mechanisms. We
226 stained for the readers in mouse ESCs, and indeed all were found to be expressed in the cytosolic
227 compartment of the cells (**Figures 4a**). Next, we knocked out each of the Ythdfs in mouse ESCs
228 using the CRISPR/Cas9 strategy (**Figure S8a**). In addition, we generated a triple-KO line,

229 Ythdf1/2/3 KO using a sequential CRISPR KO. All KO cell lines were validated by immuno-staining,
230 DNA sequencing and RNA sequencing (**Figures S8-10**).

231

232 All cell lines were viable and showed similar self-renewal ability as WT cells in mESC naïve growing
233 conditions (**Figure 4b**). In addition all cell lines expressed normal pluripotent markers (**Figure 4c**).
234 We next wanted to test their ability to undergo differentiation using *in-vivo* and *in-vitro* assays.
235 First we tested their ability to generate teratomas upon injection to immune-deficient mice
236 (**Figures 4d,e**). Interestingly, while WT and single-KO teratomas generated differentiated
237 structures containing the three germ layers, and stained for developmental markers such as
238 Foxa2 and Tuj1, triple-KO teratomas were poorly differentiated, and broadly stained for Oct4, a
239 pluripotent marker (**Figures 4d,e**), indicating their poor ability to differentiate.

240 To further examine the differentiation potential of our cells, the teratomas were disaggregated
241 and cultured in mouse ESC medium for six days. Triple-KO cells generated significantly more
242 pluripotent colonies, as shown by alkaline phosphatase staining (**Figure 4f**). In addition, embryoid
243 bodies (EBs) were generated from all our cell lines, followed by RNA extraction and qPCR. Once
244 again, differentiation markers were modestly expressed in the triple-KO EBs (**Figure 4g**),
245 indicating their poor differentiation, compared to WT and single-KO cell lines. This phenotype is
246 highly similar to the “hyper-pluripotency” phenotype which we observed previously in Mettl3-
247 KO cells (Geula et al. 2015).

248

249 **The transcriptional profile of triple-KO is distinct from WT and single-KO**

250

251 To dissect the molecular profile of single-KOs and the triple-KO, transcription profiles were
252 measured using RNA-seq from each of the cell lines (Ythdf1^{-/-}, Ythdf2^{-/-}, Ythdf3^{-/-}, Ythdf1/2/3^{-/-}).
253 In addition, we had a WT control and a positive control consisting of cells that are knocked-out
254 to Mettl3, which lack m⁶A methylation and were previously shown to be hyper-pluripotent (Geula
255 et al. 2015). Clustering the samples based on their transcriptional profile showed that while
256 single-reader-KO samples cluster together with WT samples, triple-KO samples clusters more
257 closely to Mettl3^{-/-} samples (**Figures 5a, S11a**), suggesting that single-KOs do not have a dramatic
258 effect on the transcription profile of the cells, supporting our redundancy hypothesis.

259

260 When we analyzed the number of differentially expressed genes in each of the cell lines (**Figure**
261 **5b, Table S2**), we could see that the few genes that were upregulated in the single-KOs (77 in
262 Ythdf1, 16 in Ythdf2, 37 in Ythdf3), greatly overlapped with the genes that were up-regulated in
263 triple-KO and to a lesser extent in Mettl3-KO (**Figure S11b**). Interestingly, several of the genes
264 that were upregulated in Ythdf1-KO, Ythdf3-KO and triple-KO, but not in Ythdf2-KO, were
265 significantly enriched for two-cell stage embryo genes (genes that are expressed after the first
266 division of the zygote), such as Zscan4a,c,d,f, Usp17a,b,c,e, Zfp352, Gm20767 and Tcstv1 (**Figure**

267 **5c, 5d and S11b)** (Storm et al. 2009). This suggests the even though most of Ythdfs' effects on
268 transcription are redundant, some Ythdf readers cannot always compensate for the absence of
269 the others.

270

271 To further investigate the role of the Ythdfs, their RNA binding target profile was measured in
272 three different single-Ythdf flag-tagged mESC lines using the eCLIP method (Van Nostrand et al.
273 2016). We found 201, 1995 and 146 targets that were bound by Ythdf1, Ythdf2 and Ythdf3
274 respectively. All the found targets significantly overlapped with previously published data
275 measured in human (Patil et al. 2016; Wang et al. 2015; Li et al. 2017; Niu et al. 2013; Shi et al.
276 2017) (**Figure S12a-c**). In addition, a significant part of the genes bound by the readers, also carry
277 m⁶A methylation, 75%, 70% and 63% for Ythdf1, Ythdf2 and Ythdf3 respectively (**Figure S12d**).
278 When we analyzed the common peaks between the readers, we found that the peaks bound by
279 Ythdf1 and Ythdf3 highly overlap the peaks bound by Ythdf2 (72% and 49%, respectively, **Figure**
280 **S12e, Table S3**), indicating again a possible redundancy between the readers' binding sites.
281 However, targets of Ythdf1 and Ythdf3 were not enriched for two-cell genes, which are typically
282 not expressed in mESCs, but rather to blastocyte genes that are expressed in mESCs (**Figure 12f**).
283 To investigate the roles of Ythdf1&3 in the context of two-cell genes, binding profiling needs to
284 be done in two-cell stage embryos, which is not feasible with the current technology (Van
285 Nostrand et al. 2016).

286

287 **Significant increases in m⁶A methylated mRNA half-life seen in only the triple-KO**

288

289 Previous studies proposed that m⁶A has a role in mRNA degradation (Du et al. 2016; Geula et al.
290 2015), specifically, Wang et al. (2014) suggested that Ythdf2 binds methylated transcripts and
291 directs them to mRNA decay sites. We therefore examined the decay rate in mouse ESCs, in each
292 of the single-KO and triple-KO cells. We treated the cells with actinomycin-D, and harvested RNA
293 at three time points (t=0, 4h, 8h, with duplicates of 0 and 8). We estimated transcription levels
294 using 3' poly-A RNA-seq (Geula et al. 2015), and calculated the mRNA half-life (**Methods, Table**
295 **S4**). In single-KO cells, including Ythdf2-KO, m⁶A-methylated mRNA was degraded at a similar rate
296 to non-methylated mRNA (**Figure 6a**). Only in the triple-KO cells we observed a significant
297 increase in the half-life of m⁶A methylated mRNA, compared to non-methylated mRNA, similar
298 to what was observed in Mettl3-KO (**Figure 6a**). The fact that in single-KOs there was no
299 significant effect on degradation, suggests that all of the readers have similar roles in mRNA
300 degradation and can compensate one another.

301 A previous study (Du et al. 2016) showed that Ythdf2 recruits the CCR4-NOT complex to mediate
302 accelerated deadenylation and decay. Interestingly, we observed that also Ythdf1 and Ythdf3
303 interact with CNOT1, a subunit of the CCR4-NOT complex (**Figure 6b**). Indeed, Ythdf1 and Ythdf3

304 were also shown to promote deadenylation (Du et al. 2016), further supporting the hypothesis
305 that the three readers contribute to mRNA decay, and may compensate in case of a partial loss.

306

307 Translation was also reported as a possible biological process that is affected by m⁶A methylation
308 (Shi et al. 2017). We therefore set to measure translation in our cell lines, using a ribosomal
309 footprint, which measures fragments of mRNA that are bound to a ribosome (Stern-Ginossar et
310 al. 2012). To compare translation, the ribosomal footprint was normalized by mRNA levels, giving
311 a translation efficiency level for each gene in each cell line. We observed higher translation
312 efficiency of m⁶a-methylated genes, and of Ythdf targets, compared to non-methylated genes
313 **(Figure S13b)**. However, this difference in translation efficiency was not affected by any of the
314 knockouts, suggesting that translation efficiency is not mediated directly by m⁶A methylation or
315 the Ythdfs proteins. Interestingly, a mild but significant increase in the expression of ribosomal
316 genes **(Figure 6c)** was observed in single-KO and triple-KO cell lines, an increase which is less
317 apparent in the global gene population **(Figure 6d)**.

318

319 Discussion

320

321 Previous papers have suggested that each of the Ythdf readers has unique functions (Shi et al.
322 2017; Wang et al. 2015; Li et al. 2017; Du et al. 2016; Wang et al. 2014). We propose a different
323 model, according to which, Ythdf readers have redundant functions to some extent, and show
324 multiple lines of evidence supporting this model.

325

326 Using a viability assay, we observed that there is compensation between the readers, and this
327 compensation is dosage dependent: Ythdf2 full KO or Ythdf2-heterozygotes that are also null in
328 the two other readers, are not viable. Ythdf2 heterozygote mice need at least one functional copy
329 of another Ythdf to escape total mortality **(Figure 3c)**. The fact that Ythdf2-KO has the most
330 severe lethality phenotype may be due to differences in expression patterns, as seen in oogenesis
331 and spermatogenesis **(Figures 1i, 2h)**.

332

333 The strongest evidence for Ythdf redundancy was observed in mESCs, a system in which all Ythdf
334 readers are expressed in the cytoplasmatic compartment, thus allowing examination of our
335 hypothesis. Indeed, in mESCs, we observed a redundancy in the function of Ythdf readers. Single-
336 KOs were viable, had normal self-renewal ability, expressed pluripotent markers and
337 differentiated normally upon signaling. Only in the Ythdf triple-KO did we observe an impaired
338 differentiation ability *in-vivo* and *in-vitro*, similar to the Mettl3-KO phenotype (Geula et al. 2015)).
339 In addition, only in the triple-KO did we observe a significant decrease in the degradation rate of
340 m⁶A methylated transcripts, while no change was observed in the single-KOs. Redundancy is also

341 supported by the observation that all Ythdf readers were found to bind Cnot1, part of the CCR4-
342 NOT deadenylation complex which is a suggested degradation mechanism (Du et al. 2016).

343

344 The difference in expression patterns *in-vivo* hints to us that Ythdf readers are differentially
345 regulated. Further experiments that induce the expression of Ythdf1/3 under the promoter of
346 Ythdf2 can strongly support this hypothesis. Such a system can be examined in additional
347 developmental processes such as neurogenesis or hematopoiesis. Lastly, the mechanisms that
348 regulate Ythdf expression, such as transcription factors that bind the readers, and the reader's
349 response to external signals, await further investigation.

350

351 **Abbreviation used:**

352 KO - knockout

353 WT – wild type

354 mESCs – mouse embryonic stem cells

355 EBs – embryoid bodies

356 GV – germinal vesicle

357 TE – translation efficiency

358

359 **Acknowledgments**

360 **JHH and NN are funded by** Nella and Leon Benozziyo Center for Neurological Diseases; David and Fela Shapell Family
361 Center for Genetic Disorders Research; Kekst Family Institute for Medical Genetics; Helen and Martin Kimmel
362 Institute for Stem Cell Research; Flight Attendant Medical Research Council (FAMRI); Dr. Barry Sherman Center for
363 Medicinal Chemistry; Pascal and Ilana Mantoux; Dr. Beth Rom-Rymer Stem Cell Research Fund; Edmond de
364 Rothschild Foundations; Zantker Charitable Foundation; Estate of Zvia Zeroni; European Research Council (ERC-CoG);
365 Israel Science Foundation (ISF); Minerva; Israel Cancer Research Fund (ICRF) and BSF. **We thank Schraga Schwartz,**
366 **Igor Ulitsky, Tsviya Olender, Eli Arama and Aharon Nachshon for insightful discussions and support.** We thank the
367 Weizmann Institute management and board for providing critical financial and infrastructural support.

368 **Author Contributions**

369 L.L. and J.H.H. conceived the idea for this project, designed and conducted the experiments. L.L. and N.N. wrote the
370 manuscript with J.H.H. N.N. supervised all bioinformatics analysis and analyzed the data. V.K. assisted in libraries
371 preparation, immunostaining and tissue culture. L.L., S.G. and V.K. engineered cell lines and mice strains under S.V.'s
372 supervision. S.G. assisted in teratoma formation, immunostaining and Western Blots. M.Z. assisted in mouse
373 dissection and oocyte flushing. N.M. assisted in tissue culture and Western Blots. A.A.C. assisted in oocyte staining.
374 O.M. assisted in Ribo-seq library preparation, supervised by N.S.G; J.S., A.S. and S.A. conducted the eCLIP
375 experiments. A.N. assisted in Ribo-seq analysis. S.S. analyzed the eCLIP data. G.W.Y. supervised the execution of the
376 eCLIP experiments and analyses. J.H.H. and N.N. supervised executions of experiments, adequate analysis of data,
377 and presentation of conclusions made in this paper.

378

379 **Declaration of Interests**

380 J.H.H. is an advisor to Accelta Ltd. and Biological Industries Ltd.

381

382 **Main Figure Legends**

383

384 **Figure 1. Mettl3 is essential for female mice fertility**

385 **a)** Gross morphology of Cre⁺ and Cre⁻ (control) female ovaries. Cre⁺ females show a smooth
386 shape that lacks the typical follicular morphology.

387 **b)** H&E staining of an ovary, showing a severe abnormality in Mettl3^{f/f} Vasa-Cre⁺ females.

388 **c)** Number of pups per plug produced by mating Mettl3^{f/f} Vasa-Cre⁺ females, compared to
389 Mettl3^{f/f} Vasa-Cre⁻ control females. The fathers in both cases are WT. A significant difference
390 between Cre⁺ and Cre⁻ female fertility is observed (p<0.0001, Mann-Whitney test).

391 **d)** H&E staining of ovaries, showing normal morphology in Mettl3^{f/f} Zp3-Cre⁺ ovaries.

392 **e)** Number of pups per plug produced by mating a Mettl3^{f/f} Zp3-Cre⁺ female, compared to a
393 Mettl3^{f/+} Zp3-Cre⁺ control female. The fathers in both cases are WT. A significant difference
394 between f/f and f/+ female fertility is observed (p<0.0001, Mann-Whitney test).

395 **f)** Number of oocytes per mouse produced by mating Mettl3^{f/f} Zp3-Cre⁺ females, compared to
396 Mettl3^{f/f} Zp3-Cre⁻ control females. The fathers in both cases are WT. A significant difference
397 between the number of oocytes of f/f Cre⁺ and f/f Cre⁻ is observed (p<0.0002, Mann-Whitney
398 test).

399 **g)** Top: Experimental design – Mettl3^{f/f} Zp3-Cre⁺ and Cre⁻ as control underwent hormone priming,
400 flush, fixation and staining for tubulin. Bottom: Number of oocytes observed in the different
401 stages of meiosis. In the control, most of the oocytes were in MI stage, in KO (Cre⁺) all of the
402 observed oocytes were in the GV state.

403 **h)** Staining examples of oocytes in the different stages of meiosis as observed in KO (Cre⁺) and
404 control (Cre⁻).

405 **i)** Immunostaining of Ythdf1, Ythdf2 and Ythdf3 in ICR WT oocytes after hormone priming (PMS
406 & hCG).

407

408 **Figure 2. Mettl3 and Ythdf2 are essential for male mice fertility**

409 **a)** Gross morphology of testis and epididymis of Mettl3^{f/f} Vasa-Cre⁺ and Mettl3^{f/f} Vasa-Cre⁻
410 males. Cre⁺ males show a massive decrease in testis and epididymis size compared to Cre⁻
411 control.

412 **b)** Number of pups per plug produced by Mettl3^{f/f} Vasa-Cre⁺ males, compared to Mettl3^{f/f} Vasa-
413 Cre⁻ control males. The mothers in both cases were WT. In this case there is a significant
414 hypofertility of the KO (p<0.0001, Mann-Whitney test).

415 **c)** Gross morphology of testis and epididymis of Mettl3^{f/f} Stra8-Cre⁺ and Mettl3^{f/f} Stra8-Cre⁻
416 males. Cre⁺ males show a reduced-size testis and epididymis compared to Cre⁻ control.

417 **d)** Same as in (b), for Stra8-Cre, showing a significant hypofertility of the KO (p<0.0001, Mann-
418 Whitney test).

419 **e)** Vasa, Stra8 and Prm1 are expressed during spermatogenesis, in different stages, as indicated.

- 420 **f)** Same as in (b), for Prm1-Cre, showing no significant difference between Cre⁺ and Cre⁻ male
421 fertility.
422 **g)** Number of pups per plug produced by Ythdf2^{-/-} males, compared to Ythdf2^{+/-} control males.
423 The mothers in both cases were WT. A significant difference between the fertility of KO and
424 heterozygous males is observed (p<0.0001, Mann-Whitney test).
425 **h)** Immunostaining of Ythdf1, Ythdf2 and Ythdf3 in seminiferous tubules, showing that each of
426 the proteins is expressed at different stages of spermatogenesis.

427

428 **Figure . Characterization of Ythdf1-KO, Ythdf2-KO and Ythdf3-KO mice**

- 429 **a)** Left: statistics of KO offspring received from crossing heterozygous mice from each of the
430 indicated strains (Ythdf1^{+/-}, Ythdf2^{+/-}, Ythdf3^{+/-}). Right: distribution of Ythdf2 WT, HET and KO
431 offspring in E13.5, two days postnatal (DPN), and 30 DPN (compared to expected ratios).
432 **b)** Crossing strategy for generating triple-heterozygous mice, which were further crossed, and
433 their offspring, statistics are presented in panel (c).
434 **c)** Percentage of genotypes received by crossing triple-heterozygous mice, out of 200 pups tested
435 30 DPN. Red – observed percentage, grey – expected under null assumption. No pups with
436 Ythdf2-KO genotype survived 30 DPN. In the Ythdf2^{+/-} genotype, pups with KO in either Ythdf1
437 or Ythdf3 were born at a sub-Mendelian ratio. Chi-square test p-values are indicated.
438 **d)** H&E staining showing the impaired morphology of triple-KO E7.5 embryos, compared to WT
439 control.

440

441 **Figure 4. Ythdf1, Ythdf2 and Ythdf3 are redundant in ESCs differentiation**

- 442 **a)** Immunostaining of Ythdf1, Ythdf2, and Ythdf3 in KH2 mESCs, showing a protein expression in
443 the cytosolic compartment of the cell.
444 **b)** Cell growth curve of all KO lines and WT control. Cells were grown on mouse feeders, in
445 serum/LIF conditions.
446 **c)** Brightfield and immunostaining of Nanog (green), Esrrb (red) and DAPI (blue), in KO cells
447 (single, triple and Mettl3) and WT control, showing that all cell lines express Nanog and Esrrb.
448 **d)** Teratomas generated by the KO cell line and by WT control. Single-KO cell lines show all germ
449 layers, while triple-KO teratomas as poorly differentiated.
450 **e)** Immunostaining of triple-KO and WT control with Oct4 (red), Foxa (green), Tuj1 (purple) and
451 DAPI (blue). Triple-KO contains patches of Oct4 staining, unlike WT teratomas.
452 **f)** Alkaline phosphatase (AP) staining of disassociated teratomas from Triple-KO and WT control,
453 showing a greater AP staining in the triple-KO cells.
454 **g)** RT-PCR of pluripotent genes (left) and differentiation genes (right), measured in WT and KO
455 EBs, and in WT mESCs as a control. In the triple-KO EBs, pluripotent markers are higher than the
456 control and differentiation markers are lower than the WT control.

457

458 **Figure 5. Triple-KO has a dramatic effect on gene expression**

- 459 **a)** Hierarchical clustering of samples based on Pearson correlations, showing that only single-KO
460 samples are highly similar to WT.
461 **b)** Number of differentially expressed genes in each of the KO cell line, compared to WT. Black:
462 downregulated genes. Grey: upregulated genes

- 463 c) RNA-seq and m⁶A methylation landscape of selected genes. Normalized coverage is presented.
464 Only Nanog and Dnmt3l are m⁶A-methylated. Dnmt3l, Zscan4a b d & Dppa3 are over-expressed
465 in triple-KO.
466 d) Enrichment of upregulated genes in each category, to early embryo genes (Gao et al. 2017b).
467 Genes that are upregulated in KO of Ythdf1 & 3 are specifically enriched for two-cell genes.
468 e) Normalized expression of Ythdf1,2 & 3, as measured in early mouse embryo (Gao et al. 2017b).

469
470

471 **Figure 6. All Ythdf readers interact with Cnot1 and promote mRNA degradation**

- 472 a) Half-life calculated in non-m⁶A genes (grey) and m⁶A-genes (blue), in each of the KO cell lines
473 and WT control. Only in the Triple-KO and Mettl3-KO are there a significant difference between
474 the half-life of m⁶A and non-m⁶A genes.
475 b) Flag Tag coIP of CNOT1 and HSP90 as a control, showing interactions between Ythdf1 2&3 to
476 CNOT1.
477 c) LogRatio(KO/WT) distribution of ribosomal genes (n=162), showing a significant increase in
478 their expression in the single and triple KO. * p-value < 10⁻⁶ ** p-value < 10⁻¹⁰ (paired Wilcoxon
479 test).
480 d) LogRatio(KO/WT) distribution of all genes (n=14,006), showing a non-significant difference in
481 their expression (p>=0.01, paired Wilcoxon test).

482
483

484 **Supplementary Figure Legends**

485

486 **Figure S1. Generating Ythdf1-KO, Ythdf2-KO and Ythdf3-KO *in vivo* and validation**

- 487 a) Multiple alignments of Ythdf1, Ythdf2 & Ythdf3 proteins, calculated using the Clustal
488 Omega tool. The area of YTH-domain is highlighted in red. Ythdf1-
489 Ythdf3 protein sequence similarity is 70.11%, Ythdf1-Ythdf2 is 67.15%, and Ythdf2-Ythdf3
490 is 67.78%.
491 b) Phylogenetic tree of the protein sequences of Ythdf1, Ythdf2 and Ythdf3, based on the
492 UCSC database. The three readers appear together in vertebrates, possibly due to whole
493 genome duplication.
494 c) CRISPR-Cas9 targeting strategy for knocking-out Ythdf readers *in vivo*.
495 d) KO validation using PCR, showing successful primer integration in clones #12 (Ythdf1);
496 #36, #46 (Ythdf2); #1, #3 & #4 (Ythdf3).

497

498 **Figure S2. Generating conditional knockout mice models**

- 499 a) Targeting strategy for generating Mettl3^{f/f} mice.
500 b) Crossing strategy for generating different Mettl3^{f/f} Cre+ mice.

501

502 **Figure S3. Mettl3 is essential for female mice fertility**

- 503 a) *In vitro* fertilization of Mettl3^{f/f} Zp3-Cre- control oocytes with WT sperm, leads to creation
504 of two-cell stage embryos, while the Mettl3^{f/f} Zp3-Cre+ oocytes fail to do so.

- 505 b) PCA of transcriptional profile of *Mettl3^{f/f}*Zp3-Cre- and *Mettl3^{f/f}*Zp3-Cre+ oocytes, showing
506 a distinct expression pattern.
- 507 c) Differentially expressed genes between *Mettl3^{f/f}*Zp3-Cre- and *Mettl3^{f/f}*Zp3-Cre+ oocytes,
508 along with selected enriched categories. m⁶A-methylated genes appear in bold. Ninety-
509 six genes are upregulated in the KO, and 117 are downregulated in the KO.
- 510 d) RNA-seq landscape of selected differential genes, generated with an IGV browser.
511 Normalized coverage is presented.

512

513 **Figure S4. *Mettl3* and *Ythdf2* are essential for male mice fertility**

- 514 a) H&E staining showing severe degenerative changes in the seminiferous tubules of
515 *Mettl3^{f/f}*Vasa-Cre+ and lack of sperm in the cauda epididymis.
- 516 b) H&E staining showing mild degenerative changes in the seminiferous tubules of
517 *Mettl3^{f/f}*Stra8-Cre+ and ~75% reduction in sperm quantity in the cauda epididymis,
518 compared to *Mettl3^{f/+}*Stra8-Cre+ sibling control.
- 519 c) H&E staining of seminiferous tubules showing a normal morphology in *Mettl3^{f/f}*Prm1-
520 Cre+ males.
- 521 d) H&E staining showing mild degenerative changes in the seminiferous tubules in *Ythdf2*-
522 KO males, compared to WT control.
- 523 e) Left: H&E staining in the cauda epididymis, showing severe loss of sperm in *Ythdf2*-KO
524 compared to control. Right: Brightfield of sperm extracted from the cauda epididymis of
525 KO and control, showing a severe reduction in normal sperm quantity in the KO sample,
526 compared to control.
- 527 f) Transcriptional profile of genes that are differentially expressed between *Ythdf2*-KO and
528 WT round spermatids, along with selected enriched categories. m⁶A-methylated genes
529 appear in bold; 145 downregulated in KO, and 156 upregulated in KO.

530

531 **Figure S5. *Ythdf1* knockout and *Ythdf3* knockout mice are fertile**

- 532 a) Number of pups per plug produced by mating *Ythdf1*-KO males, compared to *Ythdf1*-
533 HET males. The mothers in both cases are WT. Here there is no significant difference
534 between KO and HET male fertility (Mann-Whitney test).
- 535 b) Number of pups per plug produced by mating *Ythdf1*-KO females, compared to *Ythdf1*-
536 HET females. The fathers in both cases are WT. Here there is no significant difference
537 between KO and HET female fertility (Mann-Whitney test).
- 538 c) Number of pups per plug produced by mating *Ythdf3*-KO males, compared to *Ythdf3*-
539 HET males. The mothers in both cases are WT. Here there is no significant difference
540 between KO and HET male fertility (Mann-Whitney test).
- 541 d) Number of pups per plug produced by mating *Ythdf3*-KO females, compared to *Ythdf3*-
542 HET females. The fathers in both cases are WT. Here there is no significant difference
543 between KO and HET female fertility (Mann-Whitney test).
- 544 e) H&E staining of seminiferous tubules showing a normal morphology in *Ythdf1*-KO and
545 *Ythdf3*-KO males.
- 546 f) The morphology of *Ythdf1*-KO and *Ythdf3*-KO flushed oocytes appears to be normal,
547 similar to the *Ythdf1*-heterozygous (HET) and *Ythdf3*-HET flushed oocytes.

548

549

550 **Figure S6. Ythdf2 is essential for female mice fertility**

- 551 a) The morphology of Ythdf2-KO flushed oocytes appears to be normal, similar to the WT
552 flushed oocytes.
- 553 b) Number of pups per plug produced by mating Ythdf2^{-/-} females, compared to Ythdf2^{+/-}
554 control females. The fathers in both cases are WT. A significant difference between the
555 fertility of KO and heterozygous females is observed ($p < 0.0001$, Mann-Whitney test).
- 556 c) Transcriptional profile of genes that are differentially expressed between Ythdf2-KO and
557 WT oocytes, along with selected enriched categories; 311 downregulated in KO, and 339
558 upregulated in KO.

559

560 **Figure S7. Oocytes staining for Ythdf1, Ythdf2 and Ythdf3**

- 561 a) Immunostaining of Ythdf1, Ythdf2 and Ythdf3 in ICR WT oocytes after hormone priming
562 (PMS & hCG).
- 563 b) Immunostaining of Ythdf1, Ythdf2 and Ythdf3 in ICR WT oocytes after PMS & HCG -
564 negative control (NC), without primary antibody.
- 565 c) Immunostaining of Ythdf1, Ythdf2 and Ythdf3 in ICR WT oocytes without hormone
566 priming.

567

568 **Figure S8. Generation and validation of knockout mESC lines**

- 569 a) CRISPR-Cas9 targeting strategy for knocking out Ythdf readers in mESC cell lines.
- 570 b) Sequencing validation of the single-KO lines.
- 571 c) IGV browser view showing the missing fragments in the KO of Ythdf1, Ythdf2 & Ythdf3.

572

573 **Figure S9. Immunostaining of KO mESC lines**

- 574 a) Immunostaining of Ythdf1 (red), Nanog (green), Oct4 (purple) and DAPI (blue) in WT,
575 Ythdf1-KO, Triple-KO and Mettl3-KO cells.
- 576 b) Immunostaining of Ythdf2 (red), Nanog (green), Oct4 (purple) and DAPI (blue) in WT,
577 Ythdf2-KO, Triple-KO and Mettl3-KO cells.
- 578 c) Immunostaining of Ythdf3 (red), Nanog (green), Oct4 (purple) and DAPI (blue) in WT,
579 Ythdf3-KO, Triple-KO and Mettl3-KO cells.

580

581 **Figure S10. Morphology of knockout mESC lines**

- 582 a) Phase and alkaline phosphatase (AP) staining of WT, single-KOs and Triple-KO mESCs,
583 and phases of their EBs.

584

585 **Figure S11. Overlap of ESC signatures**

- 586 a) PCA clustering of KO and WT mESCs samples, showing that in PC1, single reader KO
587 samples are closer to WT, compared to triple-KO and Mettl3-KO.
- 588 b) Overlap between upregulated gene signatures, measured in Ythdf single-KO and triple-
589 KO, and in Mettl3-KO. Genes that are m⁶A-methylated are bold. Genes that are two-cell
590 markers are highlighted in red.

591

592 **Figure S12. CLIP data evaluation**

- 593 a) Targets of Ythdf1, Ythdf2 and Ythdf3 highly overlap targets that were published before
594 in human cancer cell lines.
595 b) Sequence logo of the GGACT containing motif which appears in 14% of YTHDF targets
596 (enrichment fold-change 1.89, $p < 1e-24$).
597 c) Distribution of Ythdf peaks in various genomic entities, showing that the three readers
598 have a tendency to bind 3' UTR, particularly Ythdf2.
599 d) Significant overlap of Ythdf targets, with m⁶a-methylated genes.
600 e) Significant overlap between Ythdf1, Ythdf2 and Ythdf3 targets
601 f) Enrichment of Ythdf targets that were identified in mESCs, to early embryo genes (Gao
602 et al. 2017), showing significant overlap with blastocyte genes.
603

604 **Figure S13. Half-life as a function of number of m⁶A peaks**

- 605 a) The half-life of m⁶A genes is plotted as a function of m⁶A peak number in the transcript,
606 showing a slight yet significant decrease in half-life (shorter), as the number of m⁶A
607 peaks increase.
608 b) Distribution of translation efficiencies of gene groups in the different samples (bottom).
609 Showing that m⁶a-methylated genes and Ythdf targets are translated in a higher
610 efficiency, consistently across samples, compared to non-methylated genes (** $p < 1e-15$,
611 * $p < 1e-6$, Kolmogorov-Smirnov test). Mettl3 and Ythdf KO hardly affect translation
612 efficiency.
613
614

615 **Supplementary Table Legends**

616
617 **Table S1.** Differentially expressed genes in gametogenesis KO experiments: Mettl3-KO
618 oocytes, and Ythdf2-KO oocytes and spermatoids, compared to matched controls.
619

620 **Table S2.** Differentially expressed genes in mESCs, that carry a single-KO (Ythdf1, Ythdf2,
621 Ythdf3 or Mettl3) or triple-KO (Ythdf1/2/3), compared to WT controls.
622

623 **Table S3.** eCLIP binding targets of Ythdf1, Ythdf2 and Ythdf3, measured in mESCs.
624

625 **Table S4.** Normalized expressed along with transcript half-life, calculated for each gene
626 in the single-KO (Ythdf1, Ythdf2, Ythdf3), triple-KO Ythdf1/2/3, and WT control.
627
628

629 **Bibliography**

- 630
631 Bailey AS, Batista PJ, Gold RS, Grace Chen Y, de Rooij DG, Chang HY, Fuller MT. 2017. The
632 conserved RNA helicase YTHDC2 regulates the transition from proliferation to
633 differentiation in the germline. *Elife* **6**: E26116.
634 Dominissini D, Moshitch-Moshkovitz S, Schwartz S, Salmon-Divon M, Ungar L, Osenberg S,
635 Cesarkas K, Jacob-Hirsch J, Amariglio N, Kupiec M, et al. 2012. Topology of the human and

- 636 mouse m6A RNA methylomes revealed by m6A-seq. *Nature* **485**: 201–206.
637 <http://www.ncbi.nlm.nih.gov/pubmed/22575960> (Accessed September 24, 2019).
- 638 Du H, Zhao Y, He J, Zhang Y, Xi H, Liu M, Ma J, Wu L. 2016. YTHDF2 destabilizes m6A-containing
639 RNA through direct recruitment of the CCR4-NOT deadenylase complex. *Nat Commun* **7**:
640 12626.
- 641 Gao LL, Zhou CX, Zhang XL, Liu P, Jin Z, Zhu GY, Ma Y, Li J, Yang ZX, Zhang D. 2017a. ZP3 is
642 Required for Germinal Vesicle Breakdown in Mouse Oocyte Meiosis. *Sci Rep* **7**: 41272.
- 643 Gao Y, Liu X, Tang B, Li C, Kou Z, Li L, Liu W, Wu Y, Kou X, Li J, et al. 2017b. Protein Expression
644 Landscape of Mouse Embryos during Pre-implantation Development. *Cell Rep* **21**: 3957–
645 3969.
- 646 Garcia-Campos MA, Edelheit S, Toth U, Safra M, Shachar R, Viukov S, Winkler R, Nir R, Lasman L,
647 Brandis A, et al. 2019. Deciphering the “m6A Code” via Antibody-Independent Quantitative
648 Profiling. *Cell* **178**: 731–747.
- 649 Geula S, Moshitch-Moshkovitz S, Dominissini D, Mansour AA, Kol N, Salmon-Divon M,
650 Hershkovitz V, Peer E, Mor N, Manor YS, et al. 2015. m⁶A mRNA methylation facilitates
651 resolution of naïve pluripotency toward differentiation. *Science* (80-) **347**.
- 652 Hartmann AM, Nayler O, Schwaiger FW, Obermeier A, Stamm S. 1999. The interaction and
653 colocalization of Sam68 with the splicing-associated factor YT521-B in nuclear dots is
654 regulated by the Src family kinase p59(fyn). *Mol Biol Cell* **10**: 3909–26.
- 655 Heck AM, Wilusz CJ. 2019. Small changes, big implications: The impact of m6A RNA methylation
656 on gene expression in pluripotency and development. *Biochim Biophys Acta - Gene Regul*
657 *Mech* **1862**: 194402.
- 658 Hsu PJ, Zhu Y, Ma H, Guo Y, Shi X, Liu Y, Qi M, Lu Z, Shi H, Wang J, et al. 2017. Ythdc2 is an N6 -
659 methyladenosine binding protein that regulates mammalian spermatogenesis. *Cell Res* **27**:
660 1115–1127.
- 661 Huang T, Liu Z, Zheng Y, Feng T, Gao Q, Zeng W. 2020. YTHDF2 promotes spermatogonial
662 adhesion through modulating MMPs decay via m6A / mRNA pathway. *Cell Death Dis* **11**:
663 37.
- 664 Ivanova I, Much C, Di Giacomo M, Azzi C, Morgan M, Moreira PN, Monahan J, Carrieri C, Enright
665 AJ, O’Carroll D. 2017. The RNA m6A Reader YTHDF2 Is Essential for the Post-transcriptional
666 Regulation of the Maternal Transcriptome and Oocyte Competence. *Mol Cell* **67**: 1059–
667 1067.
- 668 Jain D, Puno MR, Meydan C, Lailier N, Mason CE, Lima CD, Anderson K V., Keeney S. 2018. Ketu
669 mutant mice uncover an essential meiotic function for the ancient RNA helicase YTHDC2.
670 *Elife* **7**: E30919.
- 671 Jia G, Fu Y, Zhao X, Dai Q, Zheng G, Yang Y, Yi C, Lindahl T, Pan T, Yang YG, et al. 2011. N6-
672 Methyladenosine in nuclear RNA is a major substrate of the obesity-associated FTO. *Nat*
673 *Chem Biol* **7**: 885–7.
- 674 Kan L, Grozhik A V., Vedanayagam J, Patil DP, Pang N, Lim KS, Huang YC, Joseph B, Lin CJ, Despic
675 V, et al. 2017. The m6A pathway facilitates sex determination in Drosophila. *Nat Commun*
676 **8**: 15737.
- 677 Kasowitz SD, Ma J, Anderson SJ, Leu NA, Xu Y, Gregory BD, Schultz RM, Wang PJ. 2018. Nuclear
678 m6A reader YTHDC1 regulates alternative polyadenylation and splicing during mouse
679 oocyte development. *PLoS Genet* **14**: e1007412.

- 680 Lasman, L, Hanna, JH, Novershtern N. 2020. Role of m6A in Embryonic Stem Cell Differentiation
681 and in Gametogenesis. *Epigenomes* **4**.
- 682 Lee H, Bao S, Qian Y, Geula S, Leslie J, Zhang C, Hanna JH, Ding L. 2019. Stage-specific
683 requirement for Mettl3-dependent m6A mRNA methylation during haematopoietic stem
684 cell differentiation. *Nat Cell Biol* **21**: 700–709.
- 685 Li A, Chen YS, Ping XL, Yang X, Xiao W, Yang Y, Sun HY, Zhu Q, Baidya P, Wang X, et al. 2017.
686 Cytoplasmic m6A reader YTHDF3 promotes mRNA translation. *Cell Res*.
- 687 Li M, Zhao X, Wang W, Shi H, Pan Q, Lu Z, Perez SP, Suganthan R, He C, Bjørås M, et al. 2018.
688 Ythdf2-mediated m6A mRNA clearance modulates neural development in mice. *Genome*
689 *Biol* **19**: 69.
- 690 Lin Z, Hsu PJ, Xing X, Fang J, Lu Z, Zou Q, Zhang KJ, Zhang X, Zhou Y, Zhang T, et al. 2017. Mettl3-
691 /Mettl14-mediated mRNA N6-methyladenosine modulates murine spermatogenesis. *Cell*
692 *Res* **27**: 1216–1230.
- 693 Liu J, Yue Y, Han D, Wang X, Fu Y, Zhang L, Jia G, Yu M, Lu Z, Deng X, et al. 2014. A METTL3-
694 METTL14 complex mediates mammalian nuclear RNA N6-adenosine methylation. *Nat*
695 *Chem Biol* **10**: 93–5.
- 696 Meyer KD, Saletore Y, Zumbo P, Elemento O, Mason CE, Jaffrey SR. 2012. Comprehensive
697 analysis of mRNA methylation reveals enrichment in 3' UTRs and near stop codons. *Cell*
698 **149**: 1635–46.
- 699 Niu Y, Zhao X, Wu YS, Li MM, Wang XJ, Yang YG. 2013. N6-methyl-adenosine (m6A) in RNA: An
700 Old Modification with A Novel Epigenetic Function. *Genomics, Proteomics Bioinforma* **11**:
701 8–17.
- 702 O'Donnell L, O'Bryan MK. 2014. Microtubules and spermatogenesis. *Semin Cell Dev Biol* **30**: 45–
703 54.
- 704 Patil DP, Chen CK, Pickering BF, Chow A, Jackson C, Guttman M, Jaffrey SR. 2016. M6A RNA
705 methylation promotes XIST-mediated transcriptional repression. *Nature* **537**: 369–373.
- 706 Patil DP, Pickering BF, Jaffrey SR. 2018. Reading m6A in the Transcriptome: m6A-Binding
707 Proteins. *Trends Cell Biol* **28**: 113–127.
- 708 Pervaiz N, Shakeel N, Qasim A, Zehra R, Anwar S, Rana N, Xue Y, Zhang Z, Bao Y, Abbasi AA.
709 2019. Evolutionary history of the human multigene families reveals widespread gene
710 duplications throughout the history of animals. *BMC Evol Biol* **19**: 128.
- 711 Schwartz S, Agarwala SD, Mumbach MR, Jovanovic M, Mertins P, Shishkin A, Tabach Y,
712 Mikkelsen TS, Satija R, Ruvkun G, et al. 2013. High-Resolution mapping reveals a
713 conserved, widespread, dynamic mRNA methylation program in yeast meiosis. *Cell* **155**:
714 1409–21.
- 715 Shi H, Wang X, Lu Z, Zhao BS, Ma H, Hsu PJ, Liu C, He C. 2017. YTHDF3 facilitates translation and
716 decay of N6-methyladenosine-modified RNA. *Cell Res* **27**: 315–328.
- 717 Shi H, Zhang X, Weng YL, Lu Z, Liu Y, Lu Z, Li J, Hao P, Zhang Y, Zhang F, et al. 2018. m6A
718 facilitates hippocampus-dependent learning and memory through YTHDF1. *Nature* **563**:
719 249–253.
- 720 Stern-Ginossar N, Weisburd B, Michalski A, Le VTK, Hein MY, Huang SX, Ma M, Shen B, Qian SB,
721 Hengel H, et al. 2012. Decoding human cytomegalovirus. *Science (80-)* **338**: 1088–93.
- 722 Storm MP, Kumpfmüller B, Thompson B, Kolde R, Vilo J, Hummel O, Schulz H, Welham MJ.
723 2009. Characterization of the phosphoinositide 3-kinase-dependent transcriptome in

724 murine embryonic stem cells: Identification of novel regulators of pluripotency. *Stem Cells*
725 **27**: 764–75.

726 Tang C, Klukovich R, Peng H, Wang Z, Yu T, Zhang Y, Zheng H, Klungland A, Yan W. 2017.
727 ALKBH5-dependent m6A demethylation controls splicing and stability of long 3'-UTR
728 mRNAs in male germ cells. *Proc Natl Acad Sci U S A* **115**: E325–E333.

729 Van Nostrand EL, Pratt GA, Shishkin AA, Gelboin-Burkhart C, Fang MY, Sundararaman B, Blue
730 SM, Nguyen TB, Surka C, Elkins K, et al. 2016. Robust transcriptome-wide discovery of RNA-
731 binding protein binding sites with enhanced CLIP (eCLIP). *Nat Methods* **13**: 508–14.

732 Wang X, Lu Z, Gomez A, Hon GC, Yue Y, Han D, Fu Y, Parisien M, Dai Q, Jia G, et al. 2014. N 6-
733 methyladenosine-dependent regulation of messenger RNA stability. *Nature* **505**: 117–20.

734 Wang X, Zhao BS, Roundtree IA, Lu Z, Han D, Ma H, Weng X, Chen K, Shi H, He C. 2015. N6-
735 methyladenosine modulates messenger RNA translation efficiency. *Cell* **161**: 1388–99.

736 Wang Y, Li Y, Yue M, Wang J, Kumar S, Wechsler-Reya RJ, Zhang Z, Ogawa Y, Kellis M, Duester G,
737 et al. 2018. N 6-methyladenosine RNA modification regulates embryonic neural stem cell
738 self-renewal through histone modifications. *Nat Neurosci* **21**: 195–206.

739 Wei J, Liu F, Lu Z, Fei Q, Ai Y, He PC, Shi H, Cui X, Su R, Klungland A, et al. 2018. Differential m 6
740 A, m 6 A m , and m 1 A Demethylation Mediated by FTO in the Cell Nucleus and Cytoplasm.
741 *Mol Cell* **71**: 973–985.

742 Wojtas MN, Pandey RR, Mendel M, Homolka D, Sachidanandam R, Pillai RS. 2017. Regulation of
743 m 6 A Transcripts by the 3'→5' RNA Helicase YTHDC2 Is Essential for a Successful Meiotic
744 Program in the Mammalian Germline. *Mol Cell*.

745 Xia H, Zhong C, Wu X, Chen J, Tao B, Xia X, Shi M, Zhu Z, Trudeau VL, Hu W. 2018. Mettl3
746 mutation disrupts gamete maturation and reduces fertility in zebrafish. *Genetics*.

747 Xu K, Yang Y, Feng GH, Sun BF, Chen JQ, Li YF, Chen YS, Zhang XX, Wang CX, Jiang LY, et al. 2017.
748 Mettl3-mediated m 6 A regulates spermatogonial differentiation and meiosis initiation.
749 *Cell Res* **27**: 1100–1114.

750 Zheng G, Dahl JA, Niu Y, Fedorcsak P, Huang CM, Li CJ, Våggbø CB, Shi Y, Wang WL, Song SH, et
751 al. 2013. ALKBH5 Is a Mammalian RNA Demethylase that Impacts RNA Metabolism and
752 Mouse Fertility. *Mol Cell* **49**: 18–29.

753
754
755
756
757
758
759
760
761
762
763
764
765
766
767

768 Materials and Methods

769		
770		
771	Stem cell lines and cell culture	20
772	Generation of Ythdf1, Ythdf2 and Ythdf3 knock-out murine ESC lines via CRISPR/Cas9	21
773	Generation of Ythdf1, Ythdf2 and Ythdf3 knock-out mouse strains via CRISPR/Cas9	21
774	Generation of Mettl3 conditional-knockout mouse model	22
775	Generation of Mettl3 ^{flox/flox} Cre+ knock-out mice	22
776	Western blot analysis	22
777	Real Time (RT)-PCR analysis	23
778	Embryoid bodies and teratoma formation	24
779	Histology	24
780	Oocyte isolation and immunostaining	24
781	Flushing oocytes	25
782	Poking ovaries	25
783	Immunofluorescence staining	25
784	Alkaline phosphatase (AP) staining	26
785	Tetra complementation (4n) of mouse embryo	26
786	RNA stability assay	26
787	Male Germ cell isolation	26
788	RNA-seq library preparation	26
789	SMART-seq2 library preparation	27
790	Ribosome profiling & analysis	27
791	3' Poly A- RNA-sequencing Analysis	27
792	mRNA Half-Life Calculation	28
793	RNA-Seq analysis	28
794	Enrichment analysis	29
795	CLIP protocol & CLIP Analysis	29

796
797

798 Stem cell lines and cell culture

799 Maintenance of WT or Mutant murine ESCs was conducted as described previously (**Geula et al.**
800 **2015**). Briefly, mESCs expansion was carried out in 500 mL of High-glucose DMEM
801 (ThermoScientific), 15% USDA certified fetal bovine serum (FBS - Biological Industries), 1 mM L-
802 Glutamine (Biological Industries), 1% nonessential amino acids (Biological Industries), 0.1 mM β -
803 mercaptoethanol (Sigma), 1% penicillin-streptomycin (Biological Industries), 1% Sodium-
804 Pyruvate (Biological Industries), 10 μ g recombinant human LIF (Peprotech). Cells were maintained
805 in 20% O₂ conditions on irradiation inactivated mouse embryonic fibroblast (MEF) feeder cells,
806 and were passaged following 0.25% trypsinization. For RNA extraction, cells were grown on
807 Gelatin for three passages in FBS free N2B27-based media (**Gafni et al. 2013**). Briefly, 500mL of
808 N2B27 media was produced by including: 250 mL DMEM:F12 (ThermoScientific), 250 mL
809 Neurobasal (ThermoScientific), 5 mL N2 supplement (Invitrogen; 17502048 or in-house
810 prepared), 5 mL B27 supplement (Invitrogen; 17504044), 1 mM L-Glutamine (Biological
811 Industries), 1% nonessential amino acids (Biological Industries), 0.1 mM β -mercaptoethanol
812 (Sigma), penicillin-streptomycin (Biological Industries). Naïve conditions for murine ESCs included

813 10µg recombinant human LIF (Peprotech) and small-molecule inhibitors CHIR99021 (CH, 3 µM-
814 Axon Medchem) and PD0325901 (PD, 1 µM - Axon Medchem) termed 2i.

815

816 Generation of Ythdf1, Ythdf2 and Ythdf3 knock-out murine ESC lines via 817 CRISPR/Cas9

818 In order to knock out the Ythdf genes in mES cells, oligos for gRNAs were cloned into px335 vector
819 (Addgene#42335 encoding SpCas9 nickase. A pair of unique gRNA sequences for each gene were
820 chosen with the help of the Zhang Lab website <http://www.genome-engineering.org/crispr> so
821 that to leave 20-30bp offset between the CRISPR target sites. 100 µg of resulting constructs and
822 10 µg of GFP expressing vector were electroporated into V6.5 mESCs. 3 days later, GFP expressing
823 cells were sorted by FACS and seeded at low density. 9 days after seeding, colonies were picked
824 and their DNA was analyzed by High Resolution Melt assay (HRM) using MeltDoctor reagent (Life
825 Technologies). The clones that showed reduced T_m for the targeted locus were expanded and
826 sequenced to confirm mutations.

827

828 gRNA list for knocking out ythdf genes in mES cells:

829

Name	Targeting site	Sequence
mYTHDF1 gRNA1	5' region of Exon4	attccttactccctcagcg
mYTHDF1 gRNA2	5' region of Exon4	ggatagtaactggacaggta
mYTHDF2 gRNA1	Exon3	cttacttgagccacaggca
mYTHDF2 gRNA2	Exon3	acagaaccattttgtactag
mYTHDF3 gRNA1	5' region of Exon4	attggattccatattctct
mYTHDF3 gRNA2	5' region of Exon4	atatatggatctgacattgg

830

831

832 Generation of Ythdf1, Ythdf2 and Ythdf3 knock-out mouse strains via CRISPR/Cas9

833 The gRNA sequences were designed with the help of the Zhang Lab website [http://www.genome-](http://www.genome-engineering.org/crispr)
834 [engineering.org/crispr](http://www.genome-engineering.org/crispr). For Ythdf1 and Ythdf3 genes single gRNAs were chosen targeting exon3.
835 For Ythdf2 gene, we have designed a pair of gRNAs flanking exon4. The deletion of this exon
836 creates out-of-frame mutation in the coding sequence.

837 Targeting Ythdf genes in mouse single cell embryos was performed as described in (Yang et al.
838 **2014**).

839 Briefly, Cas9 and respective gRNA coding sequences tagged with T7 promoter were transcribed
840 using mMACHINE T7 ULTRA kit and MEGA shortscript T7 kit, then purified with MEGA
841 clear kit (all the kits were from Thermo Fisher Scientific). CB6F1 (C57BL/6 × BALB/c) and ICR mice
842 strains were used as embryo donors and foster mothers, respectively. Superovulated CB6F1 mice
843 (8-10 weeks old) were mated to CB6F1 stud males, and fertilized embryos were collected from
844 oviducts. Cas9 mRNAs and sgRNA (50 ng/µl) was injected into the cytoplasm of fertilized eggs
845 with well recognized pronuclei in M2 medium (Sigma). The injected zygotes were cultured in
846 KSOM with amino acids (Sigma) at 37°C under 5% CO₂ in air until blastocyst stage by 3.5 days.
847 Thereafter, 15–25 blastocysts were transferred into uterus of pseudopregnant ICR females at 2.5
848 days post coitum (dpc). Mutated animals were screened for deletions by sequencing the targeted

849 loci. *Ythdf*^{+/-} animal were backcrossed with C57BL/6 mice for 2 generations before mating in
850 order to generate *Ythdf*^{-/-} knockout mice.

851

852 gRNAs for knocking out *ythdf* genes in mice:

853

Name	Targeting site	Sequence
mYhdf1 CRISPR	Exon3	ATTGGACTGTCCAGAAAGGT
mYhdf2 5' CRISPR	Intron34	GTAAATTTTAGGACTACGGT
mYhdf2 3' CRISPR	Intron45	GTAAATTTTAGGACTACGGT
mYhdf3 CRISPR	Exon3	TTTGCTGGCTACTTAAGTA

854

855 Generation of *Mettl3* conditional-knockout mouse model

856 Stem cell lines and mice deficient for *Mettl3* were generated by targeted disruption of the
857 endogenous *Mettl3* locus via homologous recombination. The targeting strategy and construct
858 Knockout Mouse Project repository (*Mettl3*:tm1a(KOMP)Wtsi) introduced loxP sites spanning
859 the fourth exon that would result in an out-of-frame and truncated product upon deletion and
860 introduced a LacZ reporter cassette driven by the endogenous *Mettl3* promoter. 50µg DNA of
861 the targeting construct was linearized and electroporated into V6.5 ESC line that were then
862 subjected to selection with G418 (300microg/ml) After 10 d of selection, resistant clones were
863 analyzed for correct targeting. *Mettl3* f/f floxed ESC were injected to BDF1 host blastocyst and
864 chimeric mice were generated. Chimeric male mice were mated with C57BL/6 females. F1
865 offspring were screened for germline transmission by agouti coat color and validation via PCR of
866 LacZ transgene reporter. In order to remove Neomycin and lacz cassette F1 offspring were mated
867 with Rosa26-FlpE mice (Jackson Laboratory Stock#: 003946) and offspring pups were validated
868 for the removal of LacZ transgene. The mice were crossed to C57BL/6 for 3 generations before
869 used for any experiment.

870

871 Generation of *Mettl3*^{flox/flox} Cre+ knock-out mice

872 Cre+ mice were crossed with *Mettl3*^{flox/flox} mice to generate *Mettl3*^{flox/flox} Cre+ mice, as detailed
873 in **figure S2b**. The following Cre mice were used: PRM1-Cre (Jax#003328), Stra8-Cre
874 (Jax#017490), Vasa-Cre (Jax#006954) and ZP3-cre+ (Jax#003651).

875

876 Western blot analysis

877 Cells were harvested, and whole cell protein was extracted by lysis buffer, containing 150 mM
878 NaCl, 150 mM Tris-Hcl (PH = 7.4), 0.5% NP40, 1.5 mM MgCl₂, 10% Glycerol. Protein's
879 concentration was determined by BCA Kit (ThermoScientific). SDS/PAGE was performed
880 according to Laemmli and transferred to nitrocellulose membranes for immunostaining.
881 Membranes containing the transferred proteins were blocked with 5% (w/v) non-fat dried
882 skimmed milk powder in PBST, and then incubated with primary antibody in 5% BSA in PBST
883 (overnight, 4°C). Secondary antibodies used were Peroxide-conjugated AffiniPure goat anti-
884 rabbit (1:10,000, 111-035-003; Jackson ImmunoResearch). Blots were developed using
885 SuperSignal West Pico Chemiluminescent substrate (ThermoScientific, #34080). The following

886 primary antibodies were used: Ythdf2 (AVIVA SYSTEMS BIOLOGY, ARP67917_P050), Ythdf3
 887 (Santa Cruz, SC-87503), Cnot1 (Proteintech, 14276-1-A) and Hsp90 (Epitomics, 1492-1).

888

889 Real Time (RT)-PCR analysis

890 Total RNA was extracted from the cells using Trizol. 1 µg of RNA was then reverse transcribed
 891 using High-Capacity cDNA Reverse Transcription Kit (Applied Biosystems). Quantitative PCR was
 892 performed with 10ng of cDNA, in triplicates, on Vii7 platform (Applied Biosystems), using Fast
 893 SYBR® Master Mix (Applied Biosystems). Error bars indicate standard deviation of triplicate
 894 measurements for each measurement. The primers used for amplification are indicated in the
 895 primers table.

896

897 Primers list:

898

#	Primer Name	Sequence	Primer Purpose
1	Ythdf1-WT F	TAGGGAAACCCTGGGTTCCGGTC	Genotype Ythdf1-WT mice
2	Ythdf1-WT R	CGGATTGGACTGTCCAGAAAGGTAG	Genotype Ythdf1-WT mice
3	Ythdf1-KO F	TAGGGAAACCCTGGGTTCCGGTC	Genotype Ythdf1-KO mice
4	Ythdf1-KO R	CGGATTGGACTGTAGGGCTCAAAG	Genotype Ythdf1-KO mice
5	Ythdf2-WT F	AACTAGCAGCCCAGAAGGTTAAGCAGTTCAGTTATC	Genotype Ythdf2-WT mice
6	Ythdf2-WT R	GGGTGCATAAGCGTAATTGCTACTATATCC	Genotype Ythdf2-WT mice
7	Ythdf2-KO F	TGATCACCTGAACCTCACCTATACAAAACCT	Genotype Ythdf2-KO mice
8	Ythdf2-KO R	GCCAGCCCCAATTAATACTGTCTATAACT	Genotype Ythdf2-KO mice
9	Ythdf3-WT F	CAAGGTTAGCCTGGGTTACAGAAGAAA	Genotype Ythdf3-WT mice
10	Ythdf3-WT R	CTGATTGTCTGGCTACTTAAGTATGGCTC	Genotype Ythdf3-WT mice
11	Ythdf3-KO F	CAAGGTTAGCCTGGGTTACAGAAGAAA	Genotype Ythdf3-KO mice
12	Ythdf3-KO R	TTACCTGATTGTATGGCTCAAAATCATC	Genotype Ythdf3-KO mice
13	Mettl3 5'flox F	GTTGATGAAATTATCAGTACAATGGTTCTGA	Genotype Mettl3 Flox mice
14	Mettl3 5'flox R	GTAAAGAACAACCTCTGGTTATCGTCATCG	Genotype Mettl3 Flox mice
15	Prm Cre F	GCGGTCTGGCAGTAAAACTATC	Genotype Prm1 Cre mice
16	Prm Cre R	GTGAAACAGCATTGCTGTCACTT	Genotype Prm1 Cre mice
17	Stra8 Cre F	AGATGCCAGGACATCAGGAACCTG	Genotype Star8 Cre mice
18	Stra8 Cre R	ATCAGCCACACCAGACACAGAGATC	Genotype Star8 Cre mice
19	Vasa Cre F	CACGTGCAGCCGTTTAAGCCGCGT	Genotype Vasa Cre mice
20	Vasa Cre R	TTCCATTCTAAACAACACCCTGAA	Genotype Vasa Cre mice
21	Zp3 Cre F	GCGGTCTGGCAGTAAAACTATC	Genotype ZP3 Cre mice
22	Zp3 Cre R	GTGAAACAGCATTGCTGTCACTT	Genotype ZP3 Cre mice
23	Oct4 F	AGAGGATCACCTTGGGGTACA	Real Time PCR
24	Oct4 R	CGAAGCGACAGATGGTGGTC	Real Time PCR
25	Nanog F	CTCAAGTCCTGAGGCTGACA	Real Time PCR
26	Nanog R	TGAAACCTGTCTTGAGTGC	Real Time PCR
27	Sox2 F	TAGAGCTAGACTCCGGGCGATGA	Real Time PCR
28	Sox2 R	TTGCCTTAAACAAGACCACGAAA	Real Time PCR
29	Klf4 F	GCACACCTGCGAACTCACAC	Real Time PCR
30	Klf4 R	CCGTCCCAGTCACAGTGGTAA	Real Time PCR
31	Pax6 F	CGGGACTTCAGTACCAGGG	Real Time PCR

32	Pax6 R	CTTCATCCGAGTCTTCTCCG	Real Time PCR
33	Fgf5 F	CAAAGTCAATGGCTCCCACGAAG	Real Time PCR
34	Fgf5 R	CTACAATCCCCTGAGACACAGCAAATA	Real Time PCR
35	Gata6 F	CTTGCGGGCTCTATATGAACTCCAT	Real Time PCR
36	Gata6 R	TAGAAGAAGAGGAAGTAGGAGTCATAGGGACA	Real Time PCR
37	Sox17 F	GCCAAAGACGAACGCAAGCG	Real Time PCR
38	Sox17 R	TTCTCTGCCAAGGTCAACGCCT	Real Time PCR
39	Gata4 F	CACAAGATGAACGGCATCAACC	Real Time PCR
40	Gata4 R	CAGCGTGGTGGTAGTCTG	Real Time PCR
41	Otx2 F	CTTCGGGTATGGACTTGCTG	Real Time PCR
42	Otx2 R	CCTCATGAAGATGTCTGGGTAC	Real Time PCR
43	Gapdh F	AGTCAAGGCCGAGAATGGGAAG	Real Time PCR
44	Gapdh R	AAGCAGTTGGTGGTGCAGGATG	Real Time PCR
45	Actinb F	TTCTTTGCAGCTCCTTCGTT	Real Time PCR
46	Actinb R	ATGGAGGGGAATACAGCCC	Real Time PCR

899

900 Embryoid bodies and teratoma formation

901 For embryoid body (EB) *in vitro* differentiation assay, 5×10^6 ESCs were disaggregated with trypsin
902 and transferred to non-adherent suspension culture dishes, and cultured in MEF medium (DMEM
903 supplemented with 1% L-Glutamine, 1% Non-essential amino acids, 1% penicillin-streptomycin,
904 1% Sodium-Pyruvate and 15% FBS, doesn't contain Lif or 2i) for 8-10 days (time points were
905 always matched with control cells). Media replacement was carried out every 2 days.

906 For teratoma formation, 5×10^6 ESCs were injected subcutaneously to the flanks of immune
907 deficient NSG mice. After 4-6 weeks, all injected mice were sacrificed and the tumor mass
908 extracted and fixed in 4% para-formaldehyde over-night. Slides were prepared from the paraffin
909 embedded fixed tissues, which were next Hematoxylin & Eosin stained and inspected for
910 representation of all three germ layers.

911

912 Histology

913 Ovaries and testis were fixed overnight in 4% PFA overnight at 4°C. The fixed tissues were washed
914 with 25%, 50%, and 70% ethanol, embedded in paraffin, and sectioned in 4 µm thickness.

915

916 Oocyte isolation and immunostaining

917 Female mice (5-8-week old ICR) were injected with 5 i.u. of pregnant mare serum gonadotropin
918 (PMSG) (Sigma), followed by injection of 5 i.u. of human chorionic gonadotrophin (hCG) (Sigma)
919 46 hours later. Mouse oocytes were extracted from the oviduct by flushing the oviduct with M2
920 media 24 hours after hCG injection. Somatic cells were removed from the oocytes by gentle
921 pipetting in M2 media supplemented with hyaluronidase (Sigma). Oocytes were transferred to
922 an embryological watch-glass and fixed with 4% PFA EM grade (Electron Microscopy Sciences) in
923 PBS at 4°C over-night. Next, oocytes were washed 3 times in PBS (5 minutes each), permeabilized
924 in PBS with 0.3% Triton X-100 for 30 minutes, blocked with 2% normal donkey serum/0.1%
925 BSA/0.01% Tween-20 in PBS for 1 hour at room temperature (RT), and incubated over-night at
926 4°C with primary antibodies diluted in blocking solution. Oocytes were rinsed 3 times for 15
927 minutes each in blocking solution, incubated for 1 hour at room temperature with secondary

928 antibodies diluted 1:500 in blocking solution, counterstained with DAPI (1 $\mu\text{g}/\text{ml}$ in PBS) for 5
929 minutes, and washed with PBS/0.01% Tween-20 for 5 minutes 3 times. Finally, oocytes were
930 mounted in 96 well glass bottom plates for confocal imaging. The following primary antibodies
931 were used: Mouse monoclonal anti-acetylated α -Tubulin (Santa Cruz; sc-23950), Ythdf1
932 (Proteintech, 17479-1-AP), Ythdf2 (AVIVA SYSTEMS BIOLOGY, ARP67917_P050) and Ythdf3
933 (Santa Cruz, SC-87503).

934

935 Flushing oocytes

936 For the collection of oocytes by flushing, female mice were injected with 5 i.u. of pregnant mare
937 serum gonadotropin (PMSG), and after 46 hours with 5 i.u. of human chorionic gonadotropin
938 (hCG). Oocytes were extracted from the oviduct 24 hours after the hCG injection. Next, somatic
939 cells were removed from the oocytes by gentle pipetting in M2 media supplemented with
940 hyaluronidase.

941

942 Poking ovaries

943 For the collection of GV oocytes, female mice were injected with 5 i.u. of pregnant mare serum
944 gonadotropin (PMSG). After 48 hours, the ovaries were punctured in M2 media, using tweezers.
945 Next, somatic cells were removed from the oocytes by gentle pipetting in M2 media
946 supplemented with hyaluronidase.

947

948 Immunofluorescence staining

949 Cells subjected to immunofluorescence staining were washed three times with PBS and fixed
950 with 4% paraformaldehyde for 10 minutes at room temperature. Cells were then washed three
951 times with PBS and blocked for 15 min with 5% FBS in PBS containing 0.1% Triton X-100. After
952 incubation with primary antibodies (Over-night, 4°C in 5% FBS in PBS containing 0.1% Tween20)
953 cells were washed three times with PBST (PBS containing 0.1% Tween20) and incubated for one
954 hour at room temperature with fluorophore-labelled appropriate secondary antibodies
955 purchased from Jackson ImmunoResearch. Next, cells were washed and counterstained with
956 DAPI (1 $\mu\text{g}/\text{ml}$, 0215754; MP Biomedical), mounted with Shandon Immu-Mount
957 (ThermoScientific, 9990412) and imaged. All images were collected on LSM700 confocal
958 microscope and processed with Zeiss ZenDesk and Adobe Photoshop CS4 (Adobe Systems, San
959 Jose, CA).

960 Sections subjected to immunofluorescence staining were rehydrated, treated with antigen
961 retrieval, rinsed in PBS for 5 min, and permeabilized in 0.1% Triton X-100 in PBS, then blocked in
962 Blocking solution (5% normal donkey serum in PBST) in humidified chamber for 1h at RT. Slides
963 were then incubated in the appropriate primary antibody diluted in blocking solution at 4°C
964 overnight. Next, sections were washed three times in PBST, incubated with appropriate
965 fluorochrome-conjugated secondary antibodies diluted in blocking solution for one hour at room
966 temperature in the dark, washed once in PBS, counterstained with DAPI for 10 min, rinsed twice
967 in PBS, mounted with Shandon Immu-Mount (ThermoScientific, 9990412) and imaged. All images
968 were collected on LSM700 confocal microscope and processed with Zeiss ZenDesk and Adobe
969 Photoshop CS4 (Adobe Systems, San Jose, CA). The following primary antibodies were used:
970 Ythdf1 (Proteintech, 17479-1-AP), Ythdf2 (AVIVA SYSTEMS BIOLOGY, ARP67917_P050), Ythdf3

971 (Santa Cruz, SC-87503), Mettl3 (Proteintech Group 15073-1-AP), Nanog (Bethyl, A300-397A or
972 eBioscience, 14-5761), Esrrb (R&D systems, PP-H6705-00), Oct4 (Santa Cruz, SC9081 or SC5279),
973 Foxa2 (Santa Cruz, sc-6554), Tuj1 (BioLegend, 801202), Tubulin (Santa Cruz, sc-23950).
974 Throughout the manuscript, experimental and control samples were handled for staining,
975 exposure and analysis under identical conditions simultaneously to eliminate variability or bias.
976

977 Alkaline phosphatase (AP) staining

978 Alkaline phosphatase (AP) staining was performed with AP kit (Millipore SCR004) according to
979 manufacturer protocol. Briefly, cells were fixated using 4% PFA for 2 minutes, and later washed
980 with TBST. The reagents were then added to the wells, followed by an incubation of 10 minutes
981 in RT.
982

983 Tetra complementation (4n) of mouse embryo

984 4n tetraploid complementation assay was performed by flushing BDF2 embryos at the two-cell
985 stage, and subsequently allowing the embryos to develop until the blastocyst stage. At day 3.5
986 they were used for PSC micro-injection of triple-KO cell line and its corresponding WT cell line.
987 Embryos were recovered for analysis at E7.5 during development. Embryos were subjected to
988 H&E staining and were observed for developmental defects. All animal studies were conducted
989 according to the guideline and following approval by the Weizmann Institute Institutional Animal
990 Care and Use Committee.
991

992 RNA stability assay

993 For RNA stability assay 5×10^5 cells of each cell type were plated on a gelatin-coated 6 cm plate.
994 48 hours later, the media was replaced with fresh media containing 5 μ M Actinomycin-D for the
995 inhibition of mRNA transcription. Cell samples were harvested at the indicated time points (0, 4
996 and 8 hours) and total RNA was extracted using Trizol, followed by 3' Poly A-RNA-seq library
997 preparation as previously described (**Geula et al. 2015**).
998

999 Male Germ cell isolation

1000 Male germ cell populations were isolated using FACS as previously describes (**Bastos et al. 2005**;
1001 **Mahadevaiah et al. 2001**; **DiGiacomo et al. 2013**). Total RNA was isolated from FACS-sorted
1002 round spermatids, from WT control and Ythdf2 KO, using Trizol. The RNA used for RNA-seq
1003 (described below).
1004

1005 RNA-seq library preparation

1006 Total RNA was extracted from the indicated mESC cultures using Trizol and treated with DNase
1007 to avoid DNA contamination. Polyadenylated RNA was purified using Dynabeads mRNA
1008 purification kit (Invitrogen, Cat #61006), followed by library preparation using ScriptSeq v2 RNA-
1009 seq Library Preparation Kit (Illumina) according to manufacturer's instruction.
1010 Male germ cell populations were isolated using FACS as previously described (**Bastos et al. 2005**;
1011 **Mahadevaiah et al. 2001**; **DiGiacomo et al. 2013**). Total RNA was extracted using Trizol and
1012 purified using rRNA depletion (Ribo-Zero rRNA removal Kit, Illumina), followed by library

1013 preparation using ScriptSeq V2 RNA-seq Library Preparation Kit (Illumina) according to
1014 manufacturer's instruction.

1015

1016 SMART-seq2 library preparation

1017 Library was prepared according to SMART-seq2 protocol as previously described (**Picelli et al.**
1018 **2014**), with few changes: oocytes from each mouse were collected in 3 ul M2 and added to 7.9
1019 ul lysis buffer. Additional 1.1 ul of DDW was added prior to the library preparation.

1020

1021 Ribosome profiling & analysis

1022 Ribosome binding profiles in ESCs were measured in WT and KO conditions. For ribosome
1023 profiling cells were treated with Cycloheximide as previously described (McGlinicy and Ingolia
1024 2017; Ingolia et al. 2009). Cells were then lysed in lysis buffer (20mM Tris 7.5, 150mM NaCl,
1025 15mM MgCl₂, 1mM dithiothreitol) supplemented with 0.5% triton, 30 U/ml Turbo DNase
1026 (Ambion) and 100µg/ml cycloheximide, ribosome protected fragments were then generated as
1027 previously described(McGlinicy and Ingolia 2017).

1028 Reads were pre-processed by trimming their linker (sequence CTGTAGGCACCATCAAT) and
1029 polyA removal with cutadapt. Reads were aligned to mouse genome version mm10 with Bowtie
1030 aligner (parameters -v -m 16 -p 8 --max), where only uniquely aligned reads were used for
1031 further analyses. Per gene, for translation calculation, reads were counted in the coding region
1032 excluding 15 and 6 nucleotides from the beginning and end of each coding sequence (CDS),
1033 respectively (**Ingolia et al. 2009; McGlinicy and Ingolia 2017**). Translation Efficiency was
1034 measured for each gene *g* and each condition *i* as log₂(Ribogi/RNAgi). Normalized translation
1035 levels (RPKM) are available alongside the raw data, at NCBI GEO series GSE148039.

1036

1037 3' Poly A- RNA-sequencing Analysis

1038 3'-Poly A-RNA-seq was measured from WT, and KO mESCs. KO cell lines: Ythdf1^{-/-}, Ythdf2^{-/-},
1039 Ythdf3^{-/-}, Ythdf1^{-/-}Ythdf2^{-/-}Ythdf3^{-/-} and Mettl3^{-/-}. In each condition 2 biological replicates were
1040 generated, and in each replicate, three time points were measured, 0, 4 and 8 hours after
1041 Actinomycin-D induction, with two replicates of time points 0 and 8. In addition, similar 3'-Poly
1042 A-RNA-seq dataset from previous paper (**Geula et al. 2015**), including samples from mESCs and
1043 mouse Embryoid bodies (EB), of Mettl3^{-/-} and WT, measured in the same time points, was
1044 reanalyzed as described herein.

1045

Cell type	Genotype	Biological replicates	Time points in hours(repl)	Library method
mESCs	WT	2	0(2),4,8(2)	3'-polyA-seq
mESCs	Ythdf1 ^{-/-}	2	0(2),4,8(2)	3'-polyA-seq
mESCs	Ythdf2 ^{-/-}	2	0(2),4,8(2)	3'-polyA-seq
mESCs	Ythdf3 ^{-/-}	2	0(2),4,8(2)	3'-polyA-seq
mESCs	Ythdf1 ^{-/-} 2 ^{-/-} 3 ^{-/-}	2	0(2),4,8(2)	3'-polyA-seq
mESCs	WT	2	0,4,8	3'-polyA-seq
mESCs	Mettl3 ^{-/-}	2	0,4,8	3'-polyA-seq
EBs	WT	1	0,4,8	3'-polyA-seq

EBs	Mettl3 ^{-/-}	1	0,4,8	3'-polyA-seq
-----	-----------------------	---	-------	--------------

1046

1047 Reads were aligned to mouse genome version mm10 with Bowtie2 software (**Langmead and**
 1048 **Salzberg 2012**) using its default parameters. Gene expression levels were estimated using ESAT
 1049 software (**Derr et al. 2016**), and normalized by library size of each sample (FPM, fragments per
 1050 million reads). To reduce noise, genes were filtered in each sample, to include only genes with at
 1051 least 3 positive FPM calls (2 in Geula's dataset), and at least one FPM call > 3 (0.5 in Geula's
 1052 dataset), leaving 9K-12K genes in each sample.

1053 3' polyA RNA-seq values are available alongside the raw data, at NCBI GEO series GSE148039.

1054

1055 mRNA Half-Life Calculation

1056 The half-life of all genes was calculated according to the following equation: $\ln(C_i/C_0) = -kt_i$,
 1057 where k is degradation rate, C_i is the mRNA value at time i, and t_i is the time interval in hours
 1058 (**Chen et al. 2008**). Degradation rate k was estimated for each gene and each sample, from its
 1059 levels in time points 0h, 4h, 8h (as explained above) using linear regression $\text{lm}()$ function in R, on
 1060 the log transformed levels. Half-life $t_{1/2}$ is $\ln(2)/k$, where k is the degradation rate. Genes which
 1061 had negative half-life due to slight experimental noise were ignored for the rest of the analysis.
 1062 Half-life distribution was calculated for each sample, for two groups of genes: non-m⁶A genes,
 1063 and m⁶A genes which were also bound by either Ythdf1,2 or 3 (m⁶A_YTH). P-value was calculated
 1064 using Kolmogorov-Smirnov test.

1065

1066 RNA-Seq analysis

1067 RNA sequencing was measured in mESC, spermatoids and oocytes as detailed in the table below:

1068

Cell type	Genotype	Biological replicates	Library method	Single/paired-end
mESCs	WT	2	PolyA RNA-seq	Single
mESCs	Ythdf1 ^{-/-}	2	PolyA RNA-seq	Single
mESCs	Ythdf2 ^{-/-}	2	PolyA RNA-seq	Single
mESCs	Ythdf3 ^{-/-}	2	PolyA RNA-seq	Single
mESCs	Mettl3 ^{-/-}	2	PolyA RNA-seq	Single
mESCs	Ythdf1 ^{-/-} 2 ^{-/-} 3 ^{-/-}	2	PolyA RNA-seq	Single
GV Oocytes	Mettl3 ^{f/f} Zp3-Cre-	4	SMART-seq	paired
GV Oocytes	Mettl3 ^{f/f} Zp3-Cre+	3	SMART-seq	paired
Post-GV Oocytes	Ythdf2 ^{+/-}	3	SMART-seq	paired
Post-GV Oocytes	Ythdf2 ^{-/-}	2	SMART-seq	paired
Round spermatids	Ythdf2 ^{+/+}	1	Ribo-zero RNA-seq	paired
Round spermatids	Ythdf2 ^{-/-}	2	Ribo-zero RNA-seq	paired

1069

1070 Samples were analyzed using UTAP software (**Kohen et al. 2019**): Reads were trimmed using
 1071 cutadapt (Martin 2011) (parameters: -a ADAPTER1 -a "A{10}" -a "T{10}" -A "A{10}" -A "T{10}" -

1072 times 2 -q 20 -m 25). Reads were mapped to genome mm10 using STAR (**Dobin et al. 2013**)
1073 v2.4.2a (parameters: `-alignEndsType EndToEnd, -outFilterMismatchNoverLmax 0.05, -`
1074 `twopassMode Basic`). Sample counting was done using STAR, quantifying mm10 RefSeq
1075 annotated genes. Further analysis is done for genes having minimum 5 read in at least one
1076 sample. Normalization of the counts and differential expression analysis was performed using
1077 DESeq2 (**Love et al. 2014**) with the parameters: `betaPrior=True, cooksCutoff=FALSE,`
1078 `independentFiltering=FALSE`. Raw P values were adjusted for multiple testing using the
1079 procedure of Benjamini and Hochberg. Differentially expressed genes were selected with the
1080 following parameter: `padj <= 0.05, |log2FoldChange| >= 1, baseMean >= 5`.
1081 PCA and Hierarchical clustering were generated in UTAP software
1082 The normalized expression levels are available alongside the raw data, at NCBI GEO series
1083 GSE148039.
1084

1085 Enrichment analysis

1086 Enrichment analysis was done either using GeneAnalytics tool (**Figures S3c, S4f, S6c**) (**Fuchs et**
1087 **al. 2016**), or using Fisher exact test (**Figures 5d, S12a,d**).
1088

1090 CLIP protocol & CLIP Analysis

1091
1092 Binding targets of Ythdf1, Ythdf2 and Ythdf3 were determined in mESCs using eCLIP method, as
1093 described previously (Van Nostrand et al. 2016). 291, 2061 and 306 peaks were identified
1094 respectively, mapped to 147, 1034 and 149 genes. Significance of overlap with previous targets
1095 and with m⁶A-methylated genes was estimated using Fisher's exact test (**Figure S12**). Targets
1096 were mapped to human targets in order to test overlap, as previously published targets were
1097 measured in human (Patil et al. 2016; Wang et al. 2015; Li et al. 2017; Niu et al. 2013; Shi et al.
1098 2017). Binding Motif was detected using homer software v4.9.1
1099 (<http://homer.ucsd.edu/homer/motif/>).
1100

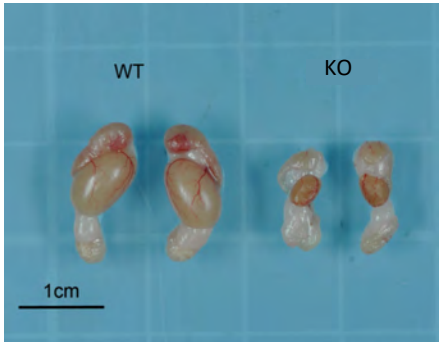
1101 Bibliography

- 1102
1103 Bastos H, Lassalle B, Chicheportiche A, Riou L, Testart J, Allemand I, Fouchet P. 2005. Flow
1104 cytometric characterization of viable meiotic and postmeiotic cells by Hoechst 33342 in
1105 mouse spermatogenesis. *Cytom Part A* **65**: 40–9.
1106 Chen CYA, Ezzeddine N, Shyu A Bin. 2008. Chapter 17 Messenger RNA Half-Life Measurements
1107 in Mammalian Cells. In *Methods in Enzymology*, pp. 335–57.
1108 Derr A, Yang C, Zilionis R, Sergushichev A, Blodgett DM, Redick S, Bortell R, Luban J, Harlan DM,
1109 Kadener S, et al. 2016. End Sequence Analysis Toolkit (ESAT) expands the extractable
1110 information from single-cell RNA-seq data. *Genome Res* **26**: 1397–1410.
1111 DiGiacomo M, Comazzetto S, Saini H, DeFazio S, Carrieri C, Morgan M, Vasiliauskaite L, Benes V,
1112 Enright AJ, O'Carroll D. 2013. Multiple Epigenetic Mechanisms and the piRNA Pathway
1113 Enforce LINE1 Silencing during Adult Spermatogenesis. *Mol Cell* **50**: 601–8.
1114 Dobin A, Davis CA, Schlesinger F, Drenkow J, Zaleski C, Jha S, Batut P, Chaisson M, Gingeras TR.

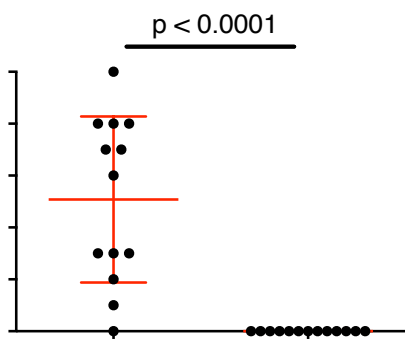
- 1115 2013. STAR: Ultrafast universal RNA-seq aligner. *Bioinformatics* **29**: 15–21.
- 1116 Fuchs SBA, Lieder I, Stelzer G, Mazor Y, Buzhor E, Kaplan S, Bogoch Y, Plaschkes I, Shitrit A,
- 1117 Rappaport N, et al. 2016. GeneAnalytics: An Integrative Gene Set Analysis Tool for Next
- 1118 Generation Sequencing, RNAseq and Microarray Data. *Omi A J Integr Biol* **20**: 139–51.
- 1119 Gafni O, Weinberger L, Mansour AA, Manor YS, Chomsky E, Ben-Yosef D, Kalma Y, Viukov S,
- 1120 Maza I, Zviran A, et al. 2013. Derivation of novel human ground state naive pluripotent
- 1121 stem cells. *Nature* **504**.
- 1122 Geula S, Moshitch-Moshkovitz S, Dominissini D, Mansour AA, Kol N, Salmon-Divon M,
- 1123 Hershkovitz V, Peer E, Mor N, Manor YS, et al. 2015. m⁶A mRNA methylation facilitates
- 1124 resolution of naïve pluripotency toward differentiation. *Science (80-)* **347**.
- 1125 Ingolia NT, Ghaemmaghami S, Newman JRS, Weissman JS. 2009. Genome-wide analysis in vivo
- 1126 of translation with nucleotide resolution using ribosome profiling. *Science (80-)* **324**: 218–
- 1127 23.
- 1128 Kohen R, Barlev J, Hornung G, Stelzer G, Feldmesser E, Kogan K, Safran M, Leshkowitz D. 2019.
- 1129 UTAP: User-friendly Transcriptome Analysis Pipeline. *BMC Bioinformatics* **20**: 154.
- 1130 Langmead B, Salzberg SL. 2012. Fast gapped-read alignment with Bowtie 2. *Nat Methods* **9**:
- 1131 357–9.
- 1132 Li A, Chen YS, Ping XL, Yang X, Xiao W, Yang Y, Sun HY, Zhu Q, Baidya P, Wang X, et al. 2017.
- 1133 Cytoplasmic m⁶A reader YTHDF3 promotes mRNA translation. *Cell Res*.
- 1134 Love MI, Huber W, Anders S. 2014. Moderated estimation of fold change and dispersion for
- 1135 RNA-seq data with DESeq2. *Genome Biol* **15**: 550.
- 1136 Mahadevaiah SK, Turner JMA, Baudat F, Rogakou EP, De Boer P, Blanco-Rodríguez J, Jasin M,
- 1137 Keeney S, Bonner WM, Burgoyne PS. 2001. Recombinational DNA double-strand breaks in
- 1138 mice precede synapsis. *Nat Genet* **27**: 271–6.
- 1139 Martin M. 2011. Cutadapt removes adapter sequences from high-throughput sequencing reads.
- 1140 *EMBnet.journal*.
- 1141 McGlincy NJ, Ingolia NT. 2017. Transcriptome-wide measurement of translation by ribosome
- 1142 profiling. *Methods* **126**: 112–129.
- 1143 Niu Y, Zhao X, Wu YS, Li MM, Wang XJ, Yang YG. 2013. N⁶-methyl-adenosine (m⁶A) in RNA: An
- 1144 Old Modification with A Novel Epigenetic Function. *Genomics, Proteomics Bioinforma* **11**:
- 1145 8–17.
- 1146 Patil DP, Chen CK, Pickering BF, Chow A, Jackson C, Guttman M, Jaffrey SR. 2016. M⁶A RNA
- 1147 methylation promotes XIST-mediated transcriptional repression. *Nature* **537**: 369–373.
- 1148 Picelli S, Faridani OR, Björklund ÅK, Winberg G, Sagasser S, Sandberg R. 2014. Full-length RNA-
- 1149 seq from single cells using Smart-seq2. *Nat Protoc* **9**: 171–81.
- 1150 Shi H, Wang X, Lu Z, Zhao BS, Ma H, Hsu PJ, Liu C, He C. 2017. YTHDF3 facilitates translation and
- 1151 decay of N⁶-methyladenosine-modified RNA. *Cell Res* **27**: 315–328.
- 1152 Van Nostrand EL, Pratt GA, Shishkin AA, Gelboin-Burkhart C, Fang MY, Sundararaman B, Blue
- 1153 SM, Nguyen TB, Surka C, Elkins K, et al. 2016. Robust transcriptome-wide discovery of RNA-
- 1154 binding protein binding sites with enhanced CLIP (eCLIP). *Nat Methods* **13**: 508–14.
- 1155 Wang X, Zhao BS, Roundtree IA, Lu Z, Han D, Ma H, Weng X, Chen K, Shi H, He C. 2015. N⁶-
- 1156 methyladenosine modulates messenger RNA translation efficiency. *Cell* **161**: 1388–99.
- 1157 Yang H, Wang H, Jaenisch R. 2014. Generating genetically modified mice using CRISPR/Cas-
- 1158 mediated genome engineering. *Nat Protoc* **9**: 1956–68.

Figure 2. Mettl3 and Ythdf2 are essential for male mice fertility

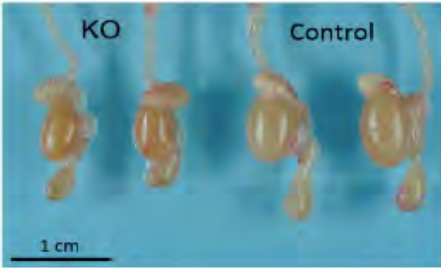
a



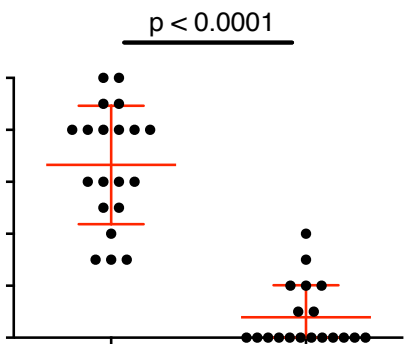
b



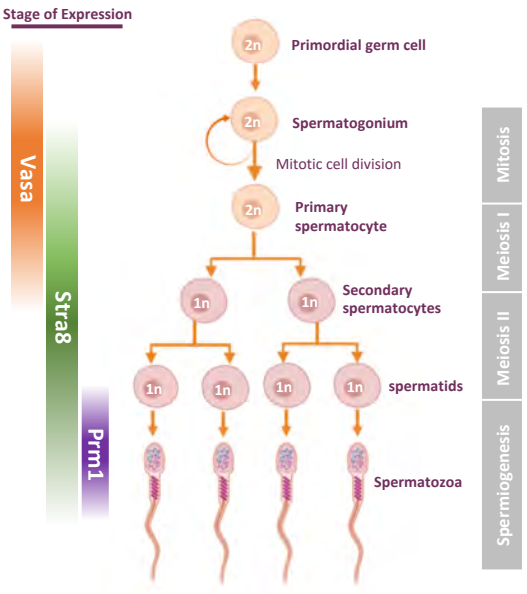
c



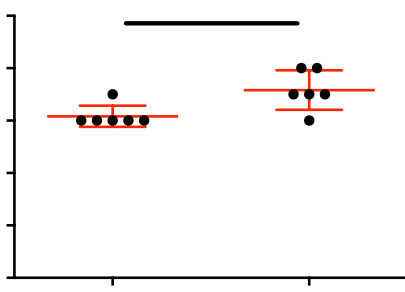
d



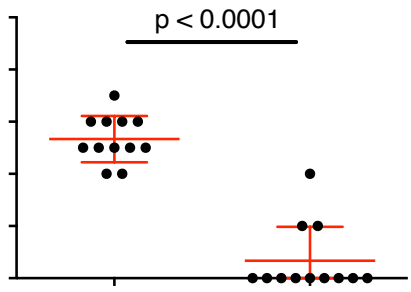
e



f



g



h

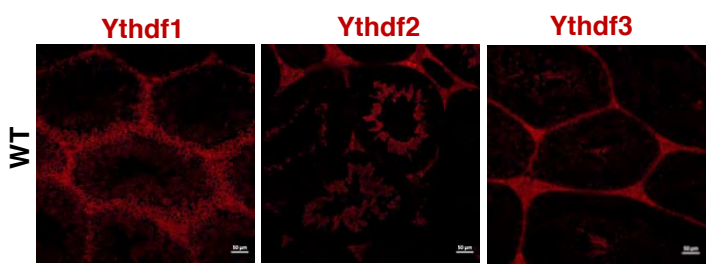
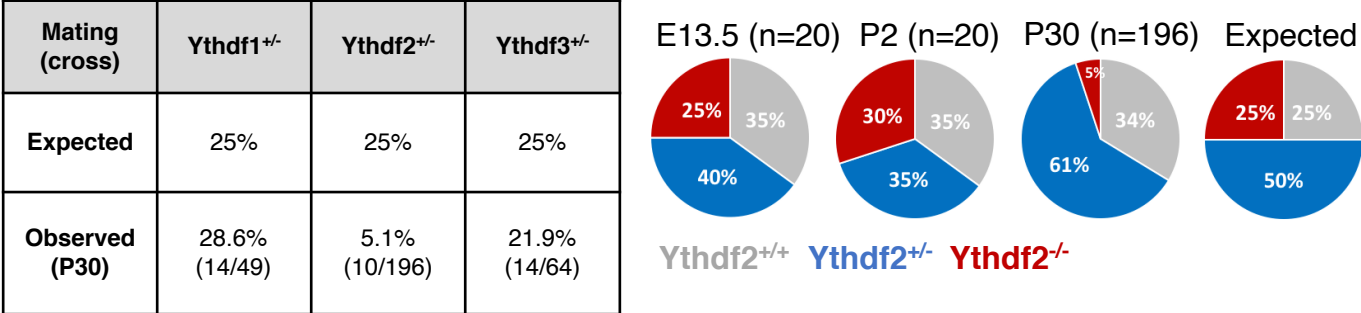
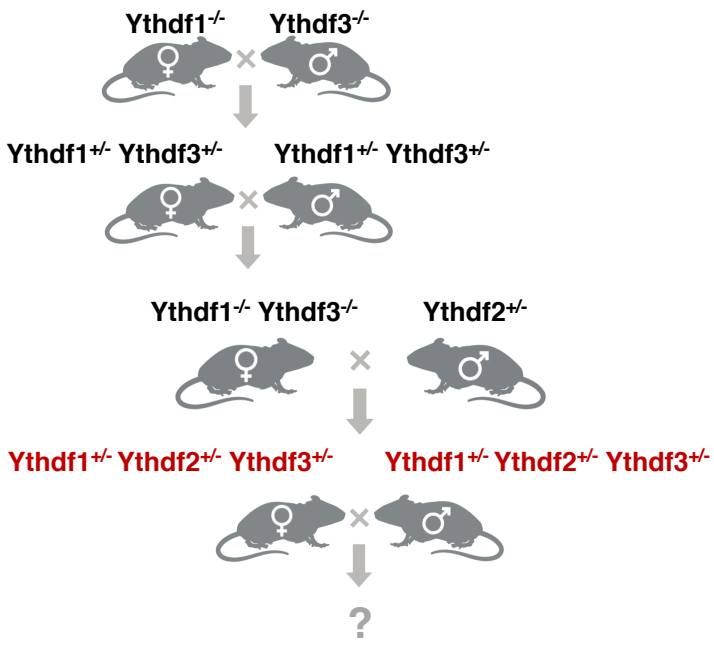


Figure 3. Characterization of Ythdf1-KO, Ythdf2-KO and Ythdf3-KO mice

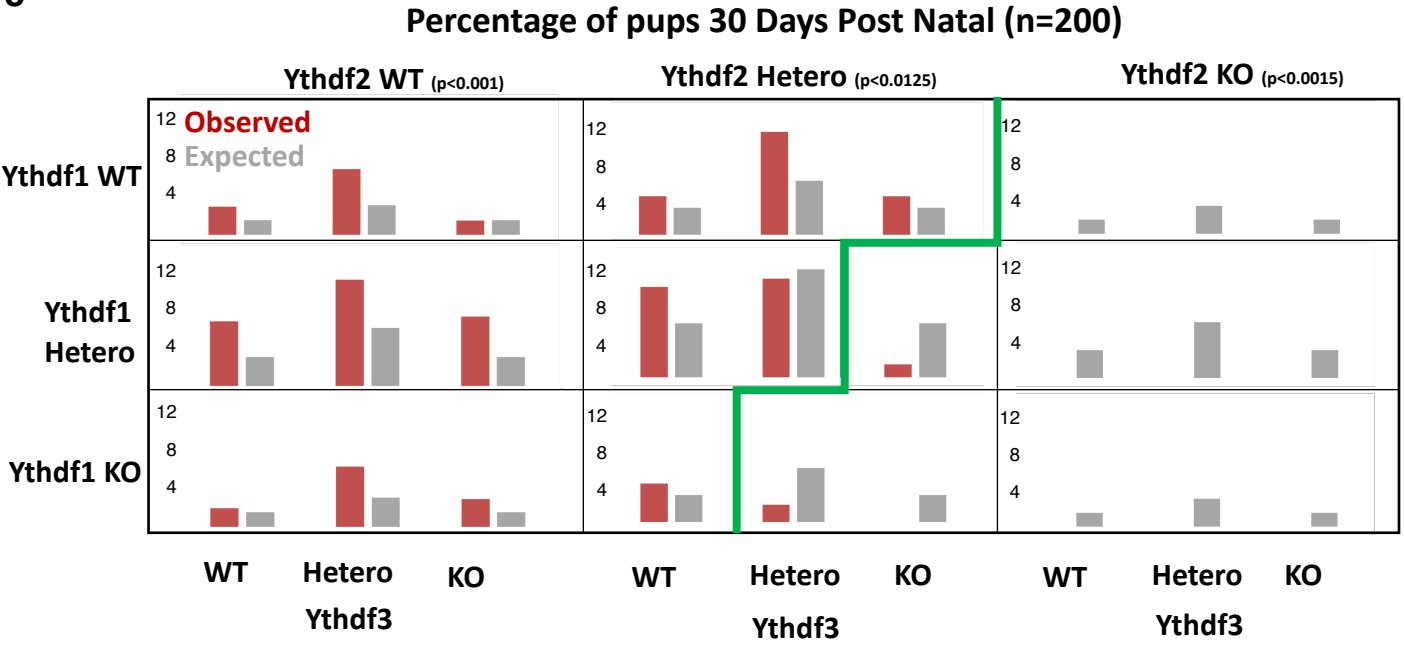
a



b



c



d

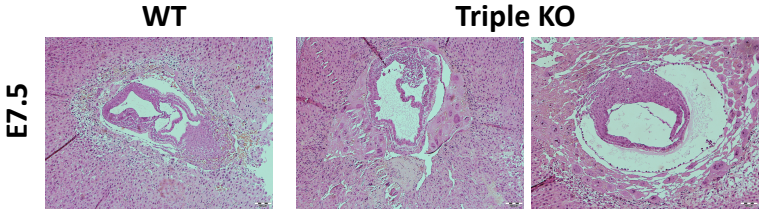


Figure 4. Ythdf1, Ythdf2 and Ythdf3 are redundant in ESCs differentiation

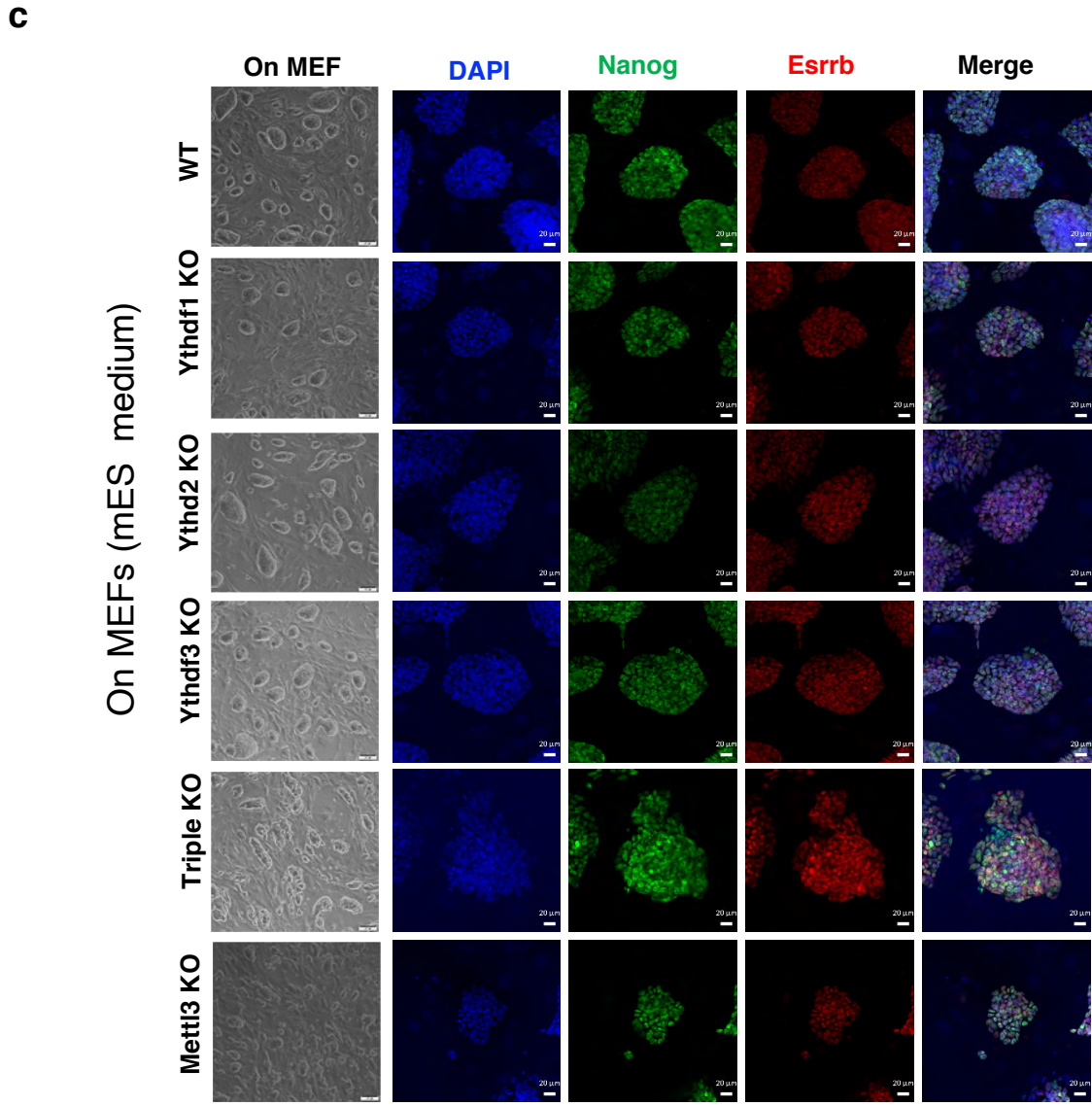
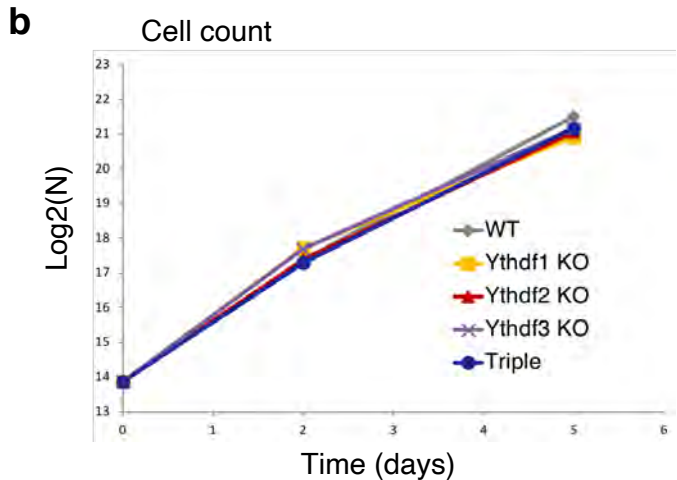
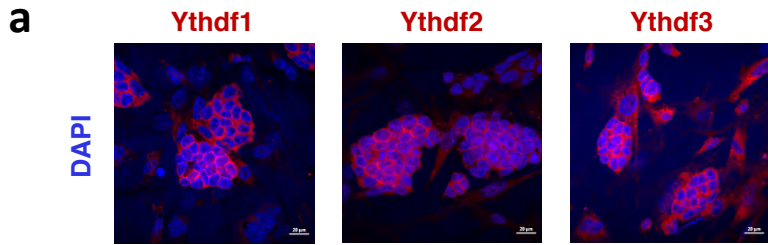


Figure 4..cont. Ythdf1, Ythdf2 and Ythdf3 are redundant in ESCs differentiation

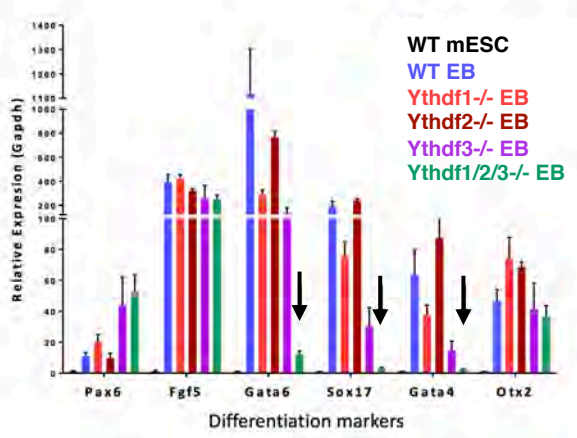
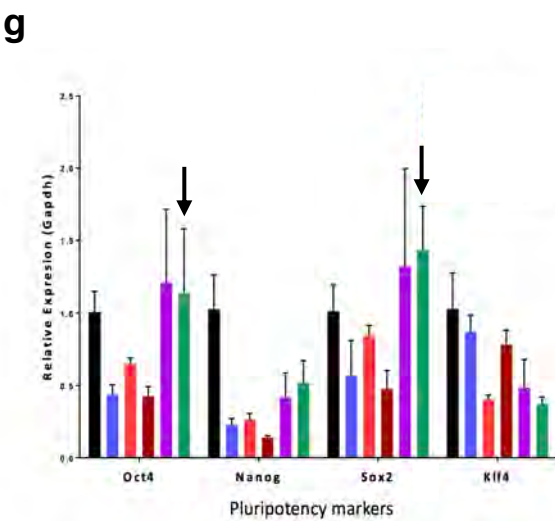
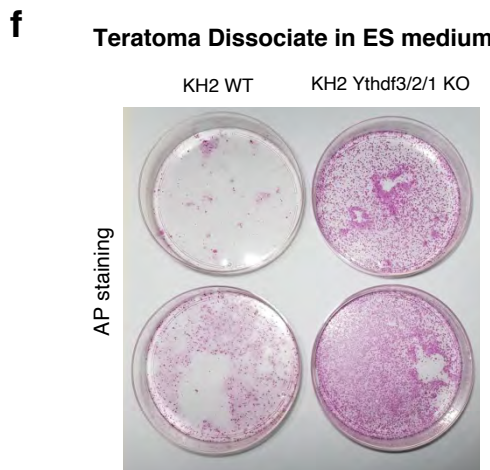
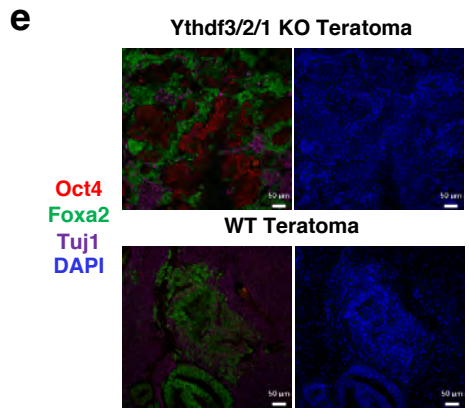
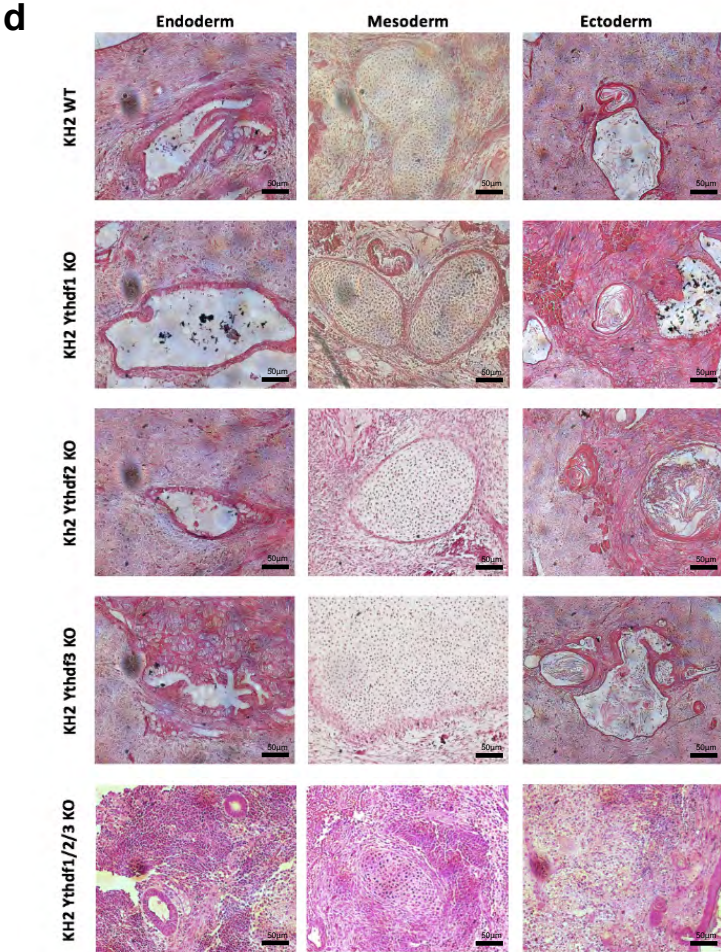


Figure 5. Triple-KO has a dramatic effect on gene expression

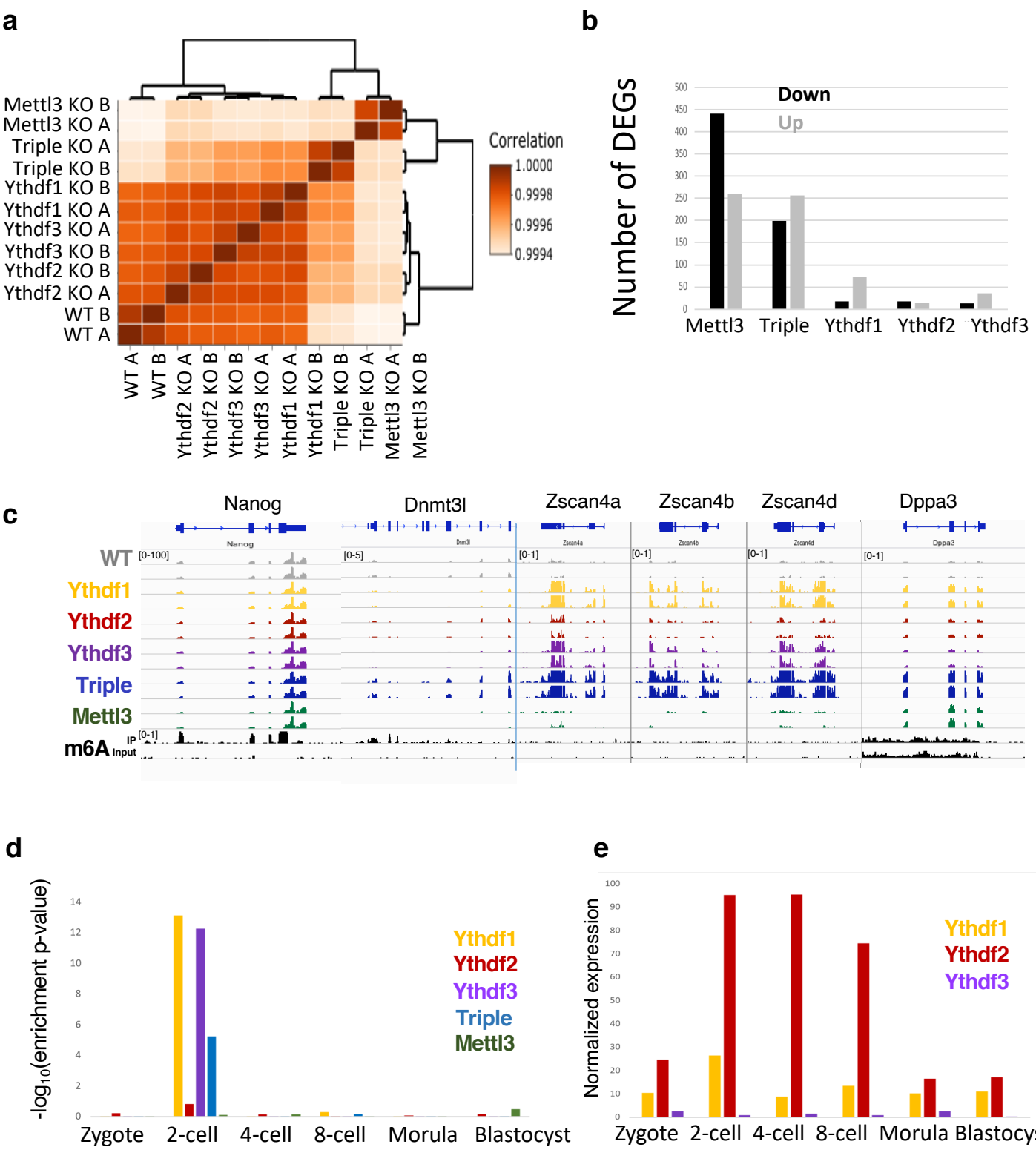
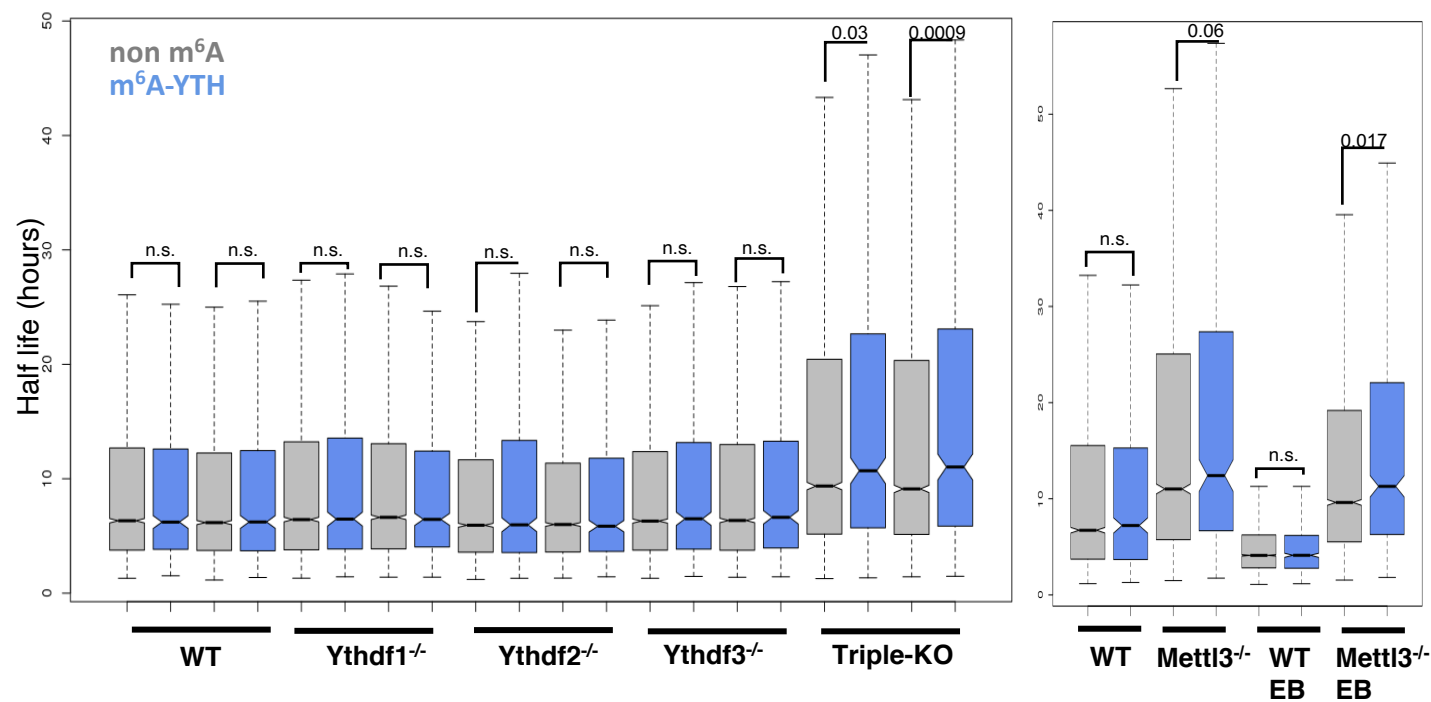
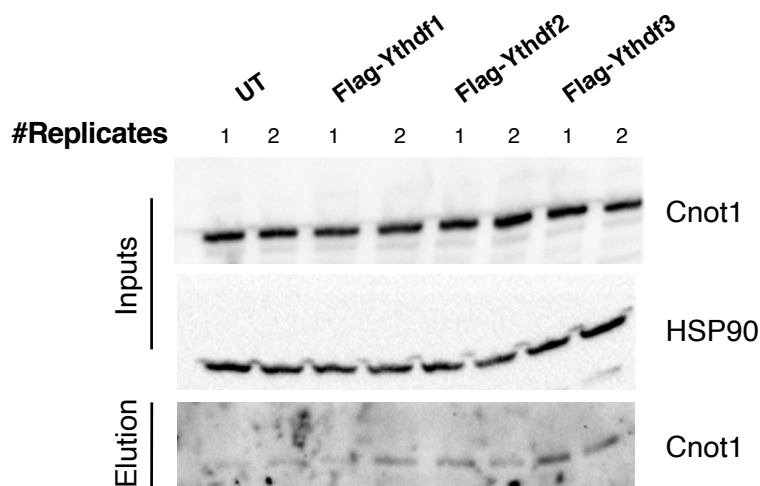


Figure 6. Single and Triple KOs in degradation & translation

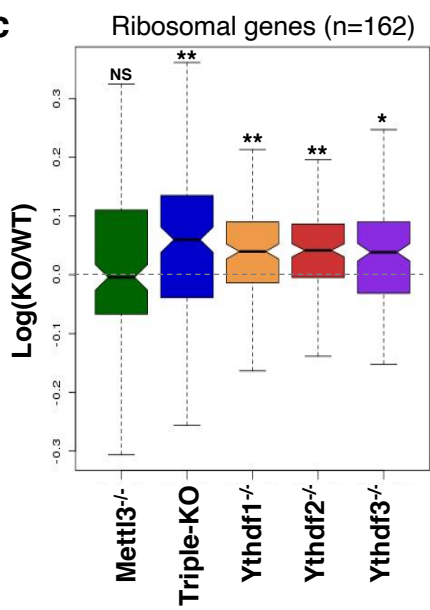
a



b



c



d

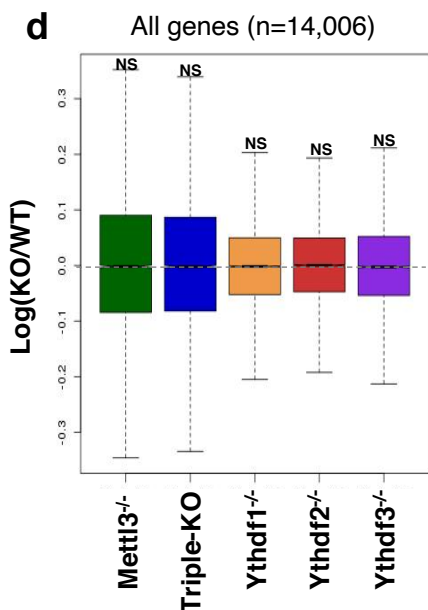


Figure S1. Generating Ythdf1-KO, Ythdf2-KO and Ythdf3-KO *in vivo* and validation

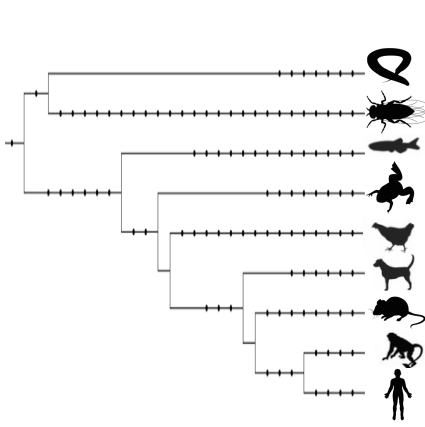
a

```

sp|Q11Y7|YTHD_MOUSE MSASSLLRQ--KPKQQQNVVQNGSVHQKGLKDDDFEFLYLPQARPHRYATNMSDEYLP 58
sp|P59326|YTHD_MOUSE MSATSV-DQ-KTYQDNVYVQGLRQDAVNDNDFEFLDQGNFMRVPMNSDFPLSS 58
sp|Q8BYK6|YTHD_MOUSE MSATSV-DGKPFQDQNVVYVQNGSIHQDAVNDNDFEFLDQGNFMRVPMNSDFPMS 59
.....
sp|Q11Y7|YTHD_MOUSE YTFPFIIGFYSLGEAMSTAGDTPAMFLYSYGLSNGEHLFLPAMFGQAGLGGT-PFL 117
sp|P59326|YTHD_MOUSE YTFPFIIGFYSLGEAMSTAGDTPFPIVLTLYQGLSNDRFRDADVYDQVQGLGNN--I 115
sp|Q8BYK6|YTHD_MOUSE YTFPFIIGFYSLGEAMSTAGDTPMFLTLYQGLSNDRFRDADVYDQVQGLGNYFFFL 119
.....
sp|Q11Y7|YTHD_MOUSE QHQGFVFFPFCIDFLAMONNSQQGTFSSQVSENYTAPFSLGGMIDQSAFAMETLN 177
sp|P59326|YTHD_MOUSE YQHRFFPFFRPAFAFAMTSGSQDQDQGRASVYSSYTFPSSLGATITDQAGFGDLS 175
sp|Q8BYK6|YTHD_MOUSE QHQGFVFFPFRADFTWQTSQSQDQGRASVYSSYTFPSSLGATITDQAGFGDLS 179
.....
sp|Q11Y7|YTHD_MOUSE KAPKQRTIDQGMALLGQTVASVYVYVGVGSGEITRIVASSLFPATIAFPEFA 237
sp|P59326|YTHD_MOUSE KAPKQRLHQGQGLIGVETVLA-VYFQGVVYVVALQGLVLSGQGVVQVWVDFPFT 232
sp|Q8BYK6|YTHD_MOUSE KVPGISIDIQGQGLIGDGLTA-AVYTVGTALSSGQTS-IAT-NWVFFGSAAPKPT 236
.....
sp|Q11Y7|YTHD_MOUSE SMADIASFPAKQKPLTYNG--LAGEFLPPPFIKHWIDQVWNGVPAVAPQALVON 295
sp|P59326|YTHD_MOUSE SMADIASFPAKQKPLTYNG--LAGEFLPPPFIKHWIDQVWNGVPAVAPQALVON 295
sp|Q8BYK6|YTHD_MOUSE SMADIASFPAKQKPLTYNG--LAGEFLPPPFIKHWIDQVWNGVPAVAPQALVON 296
.....
sp|Q11Y7|YTHD_MOUSE IQGPTGSPVQVQAN-SEPPVAQAVVQDQPLFPF-----PQAGLSVQQA 345
sp|P59326|YTHD_MOUSE PD-AA-PQDQVAPLQVPPFLVQ-----PQVGS-PQQ 222
sp|Q8BYK6|YTHD_MOUSE PD-TIIGQVPLI---QVPLVQVGLPQ-QQVPPVQVQVQVQVQVQVQVQVQVQV 348
.....
sp|Q11Y7|YTHD_MOUSE AQPTRVAVRNSGGGCHNGY---RGNVQVQVQVQVQVQVQVQVQVQVQVQVQV 402
sp|P59326|YTHD_MOUSE PLOPRVAVRNSKAAFQVQVQVQVQVQVQVQVQVQVQVQVQVQVQVQVQVQVQV 381
sp|Q8BYK6|YTHD_MOUSE QLRVAVRNSKAAFQVQVQVQVQVQVQVQVQVQVQVQVQVQVQVQVQVQVQV 408
.....
sp|Q11Y7|YTHD_MOUSE FDNLLRSGVFFIIFSSDDIRHSIYSIMCTEKNHLLGAFVSNSSGQVPLFVSN 462
sp|P59326|YTHD_MOUSE FDNLLRSGVFFIIFSSDDIRHSIYSIMCTEKNHLLGAFVSNSSGQVPLFVSN 461
sp|Q8BYK6|YTHD_MOUSE FDNLLRSGVFFIIFSSDDIRHSIYSIMCTEKNHLLGAFVSNSSGQVPLFVSN 468
.....
sp|Q11Y7|YTHD_MOUSE GSGRFQVARNISAVYVTCAGVNSQVWQVDFVWVIFVDFVNSQLRHSILENDSFP 522
sp|P59326|YTHD_MOUSE GSGRFQVARNISAVYVTCAGVNSQVWQVDFVWVIFVDFVNSQLRHSILENDSFP 501
sp|Q8BYK6|YTHD_MOUSE GSGRFQVARNISAVYVTCAGVNSQVWQVDFVWVIFVDFVNSQLRHSILENDSFP 528
.....
sp|Q11Y7|YTHD_MOUSE VTHSDQVPLEAIVQLSLIASVYHTSIFDFSRVYEQEEREVVRHQGQGS- 579
sp|P59326|YTHD_MOUSE VTHSDQVPLEAIVQLSLIASVYHTSIFDFSRVYEQEEREVVRHQGQGS- 559
sp|Q8BYK6|YTHD_MOUSE VTHSDQVPLEAIVQLSLIASVYHTSIFDFSRVYEQEEREVVRHQGQGS- 585
.....

```

b



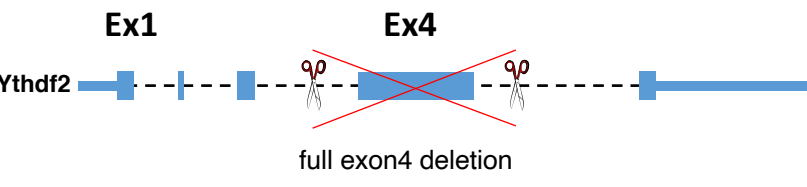
Ythdf1 Ythdf2 Ythdf3

-	-	-
+	-	-
+	+	+
+	+	+
+	+	+
+	+	+
+	+	+
+	+	+
+	+	+
+	+	+

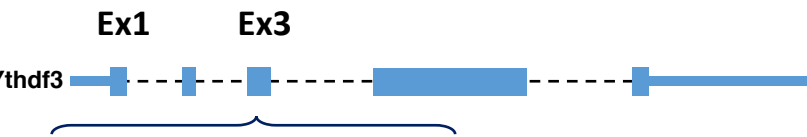
c



Mutant allele: 10bp deletion
 agccctac ~~ctttctggac~~ agtccaatccg



full exon4 deletion



Mutant allele: 14bp deletion
 aatgatg ~~attttgaccatac~~ ttaagttagc

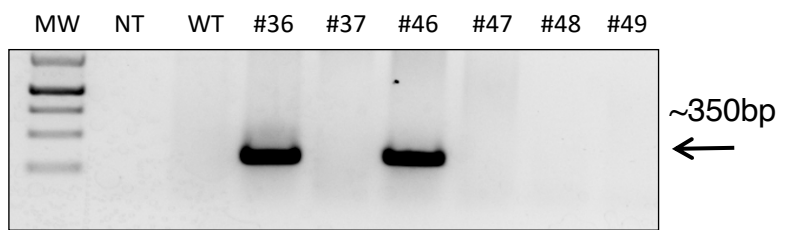
Figure S1..Cont. Generating Ythdf1-KO, Ythdf2-KO and Ythdf3-KO *in vivo* and validation

d

Ythdf1 KO primers



Ythdf2 KO primers



Ythdf3 KO primers

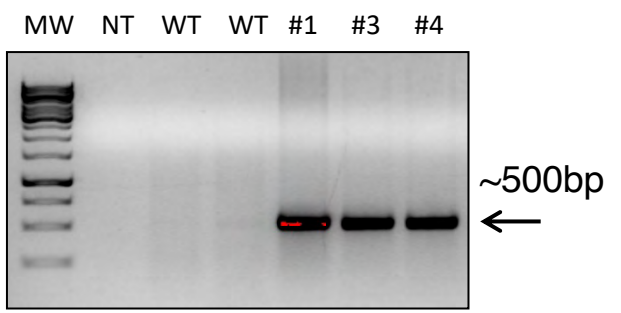
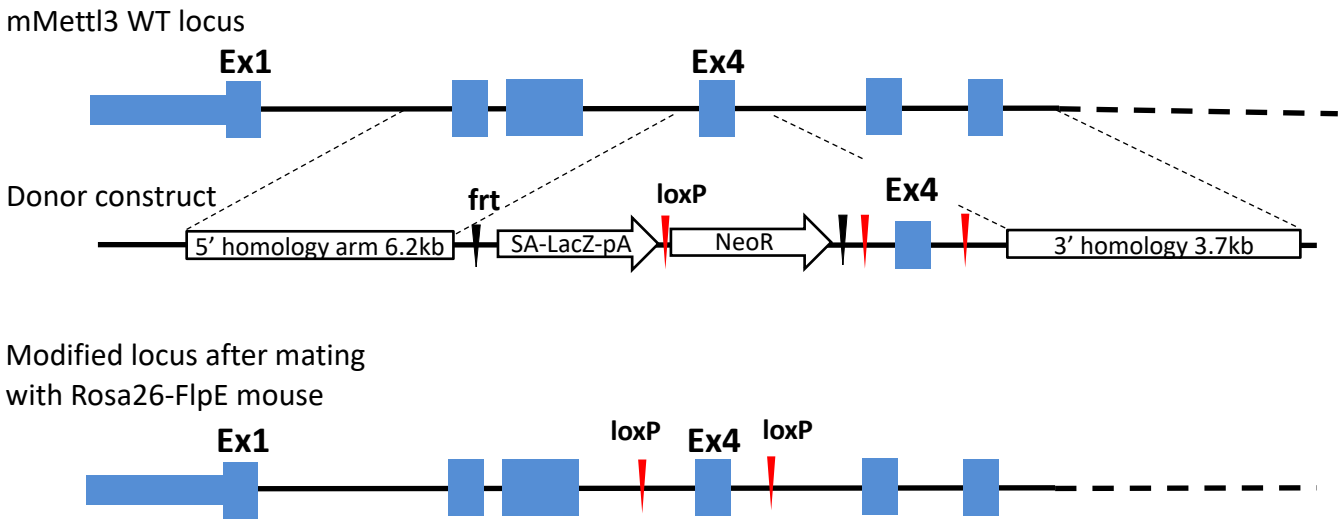


Figure S2. Generating conditional Knock-Out mice models

a



b

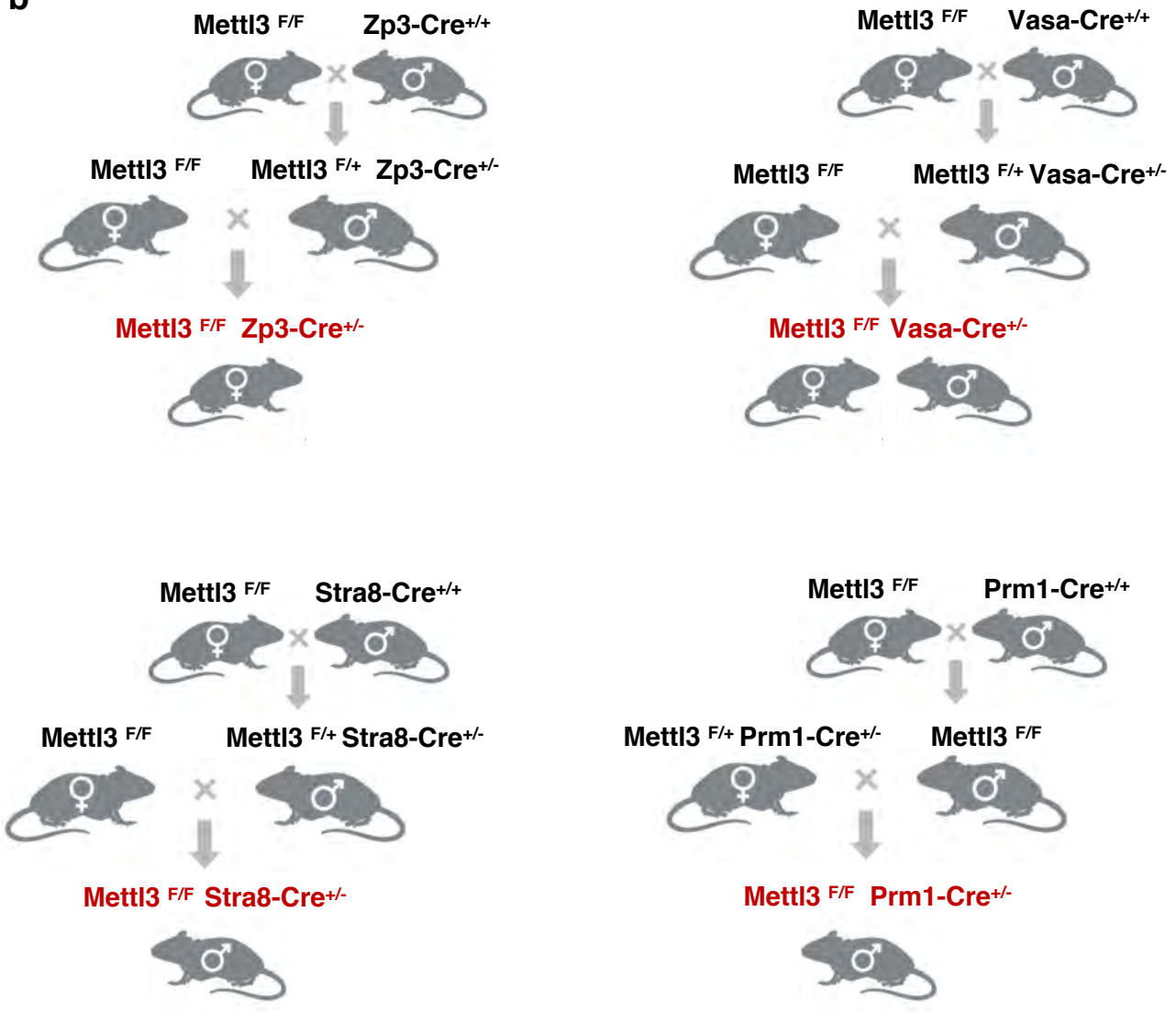
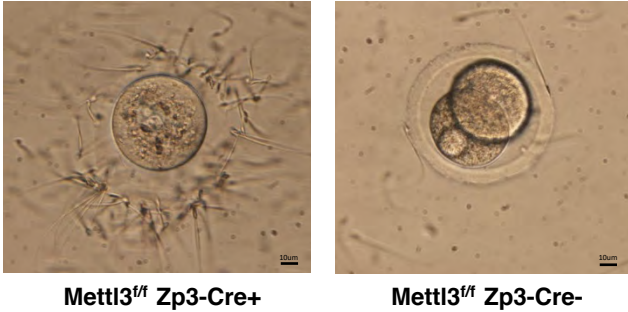


Figure S3. *Mettl3* is essential for female mice fertility

a

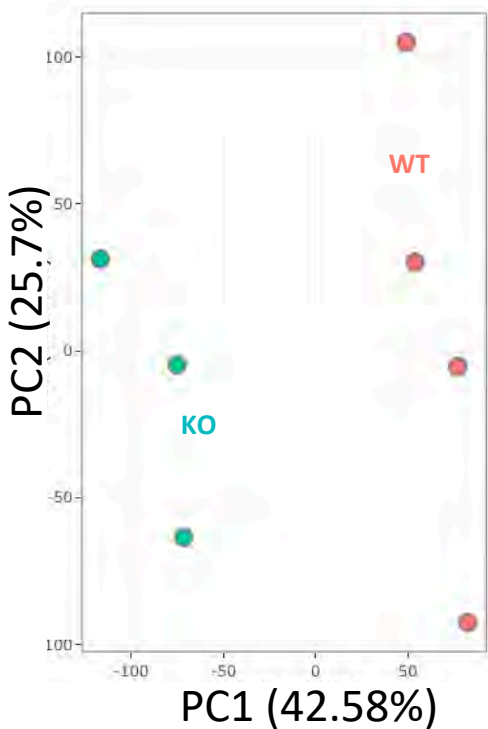
Response to fertilization



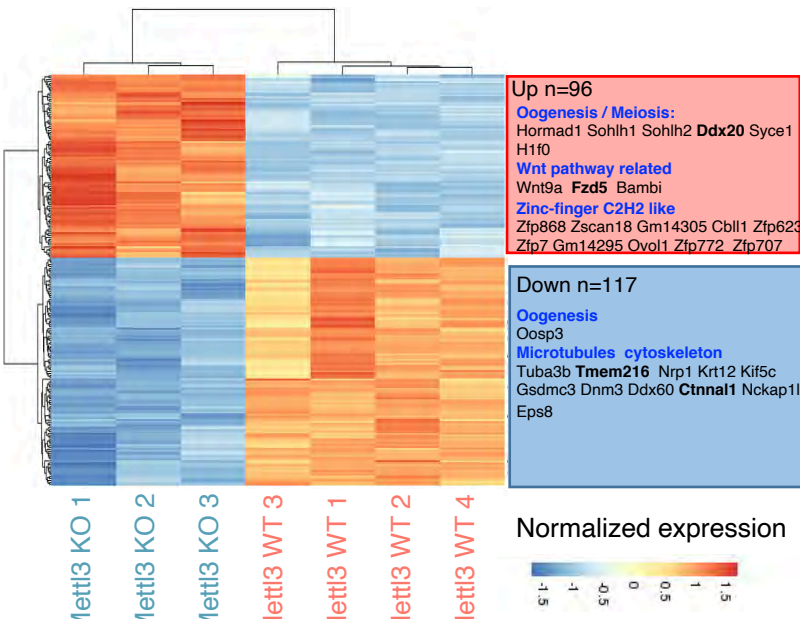
Mettl3^{ff} Zp3-Cre+

Mettl3^{ff} Zp3-Cre-

b



c



d

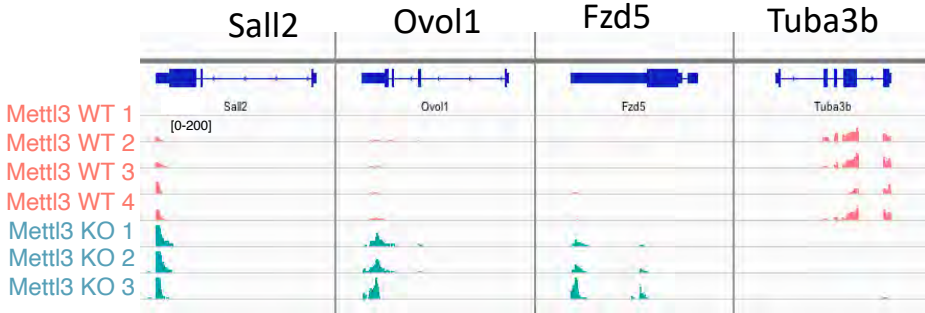


Figure S4. *Mettl3* and *Ythdf2* are essential for male mice fertility

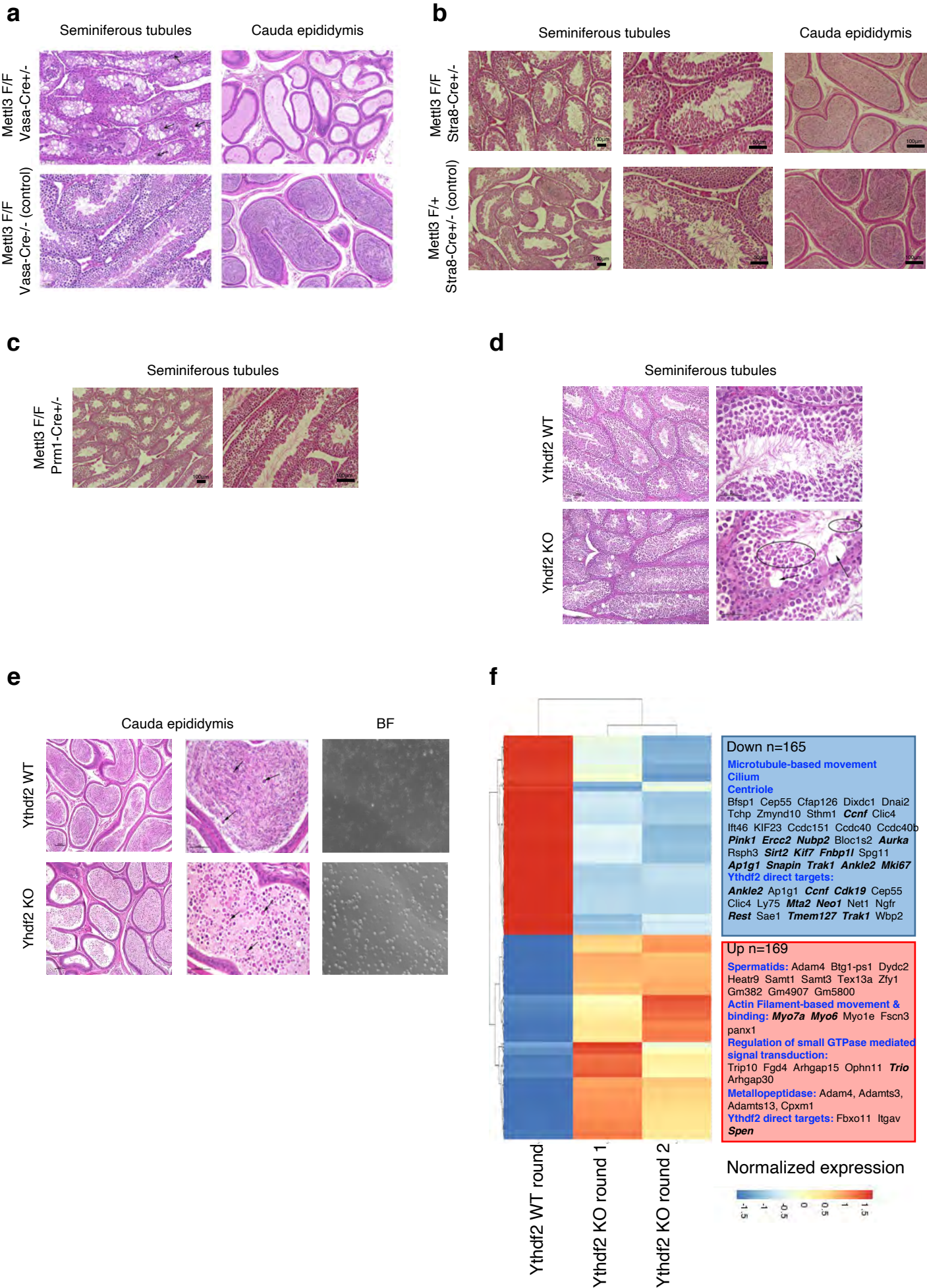


Figure S5. Ythdf1 Knock-Out and Ythdf3 Knock-Out mice are fertile

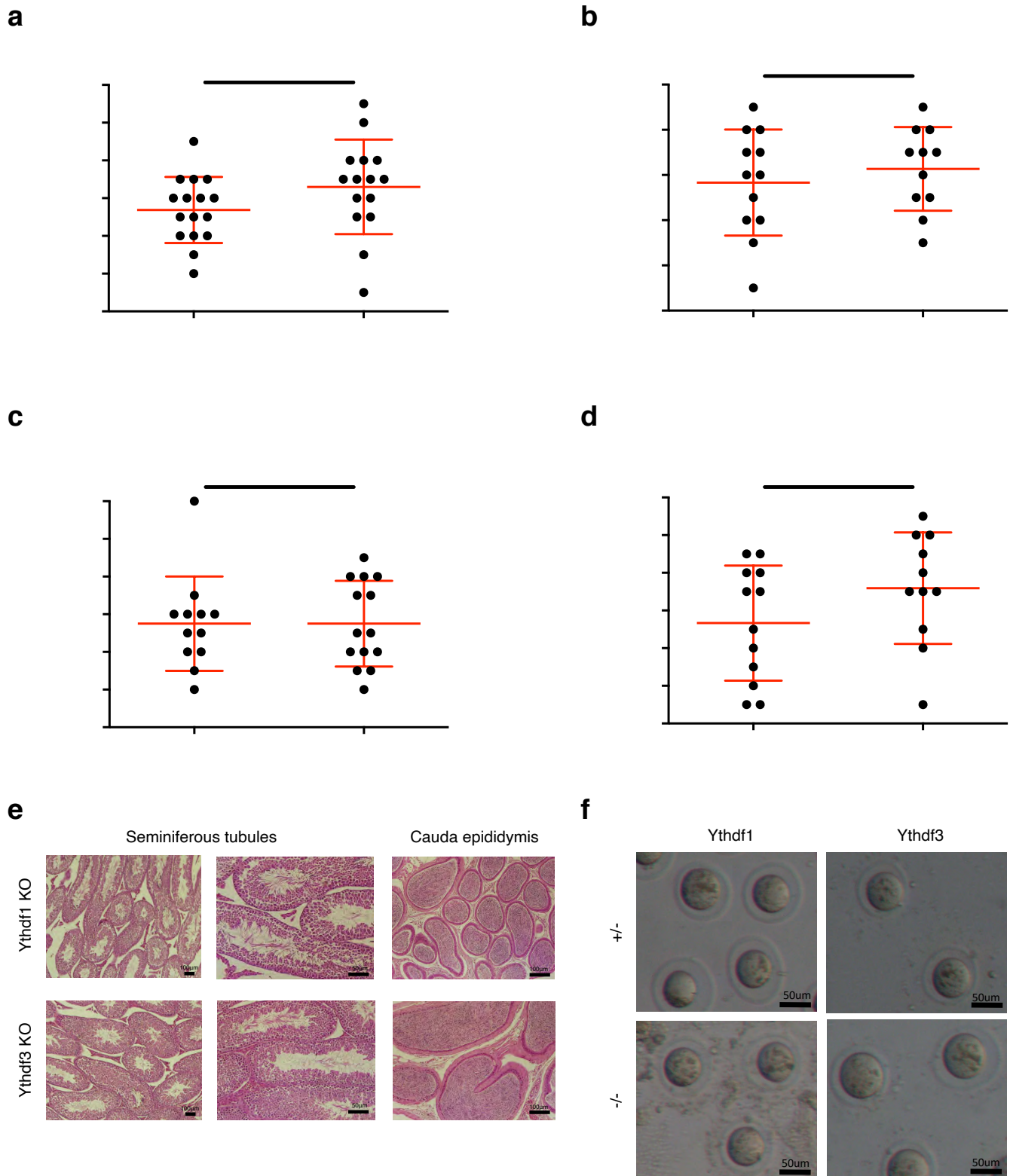
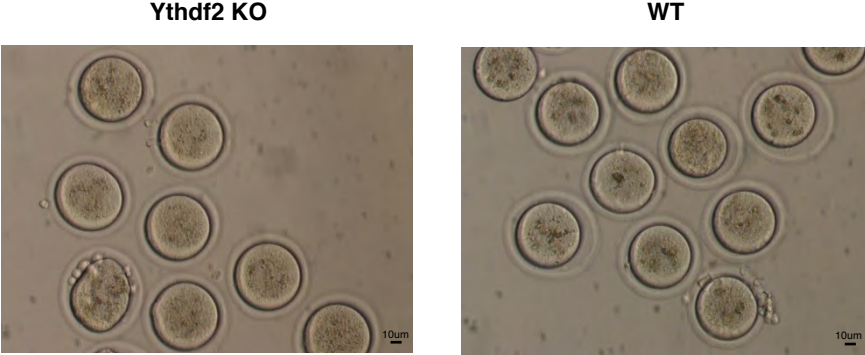
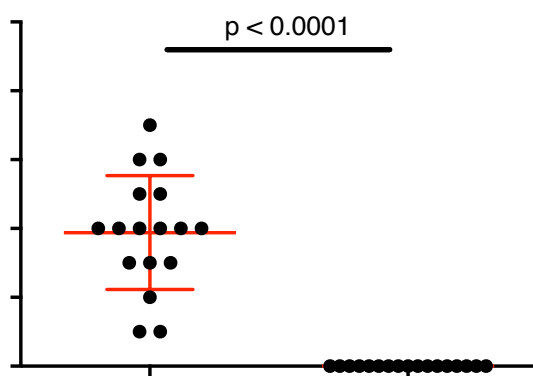


Figure S6. Ythdf2 is essential for female mice fertility

a



b



c

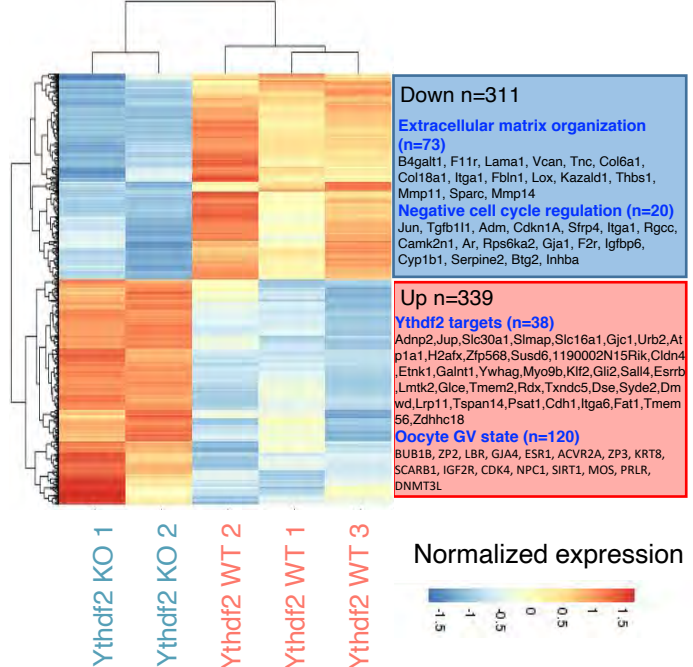


Figure S7. Oocytes staining for Ythdf1, Ythdf2 and Ythdf3

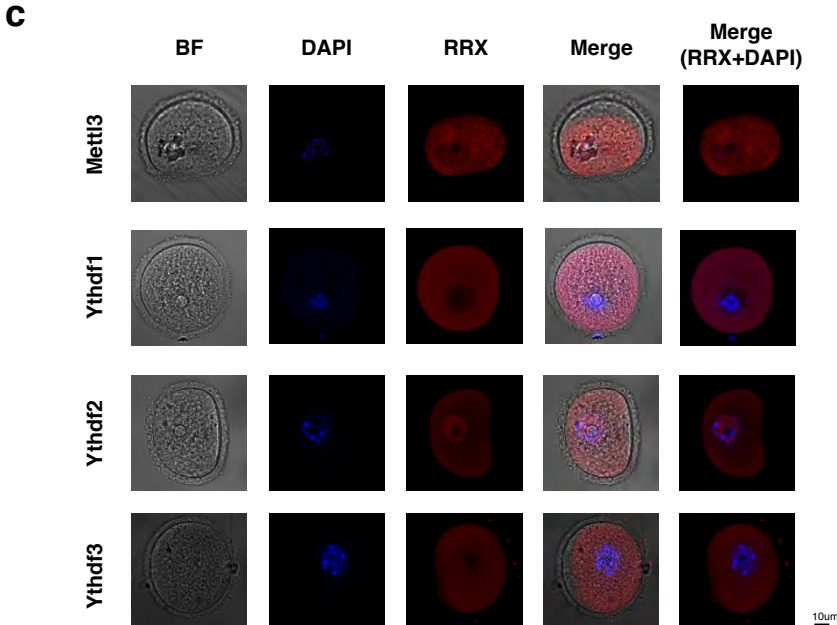
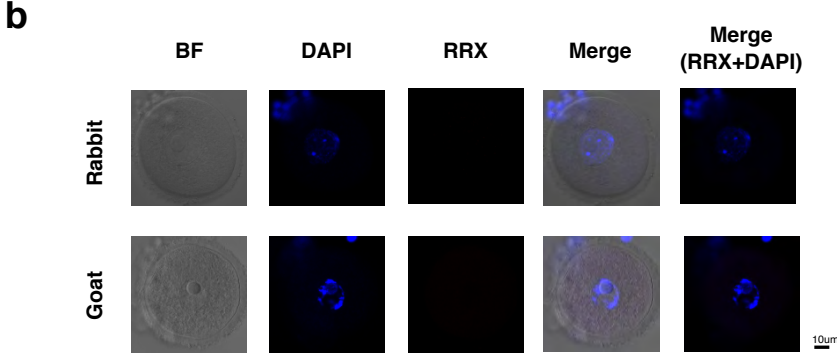
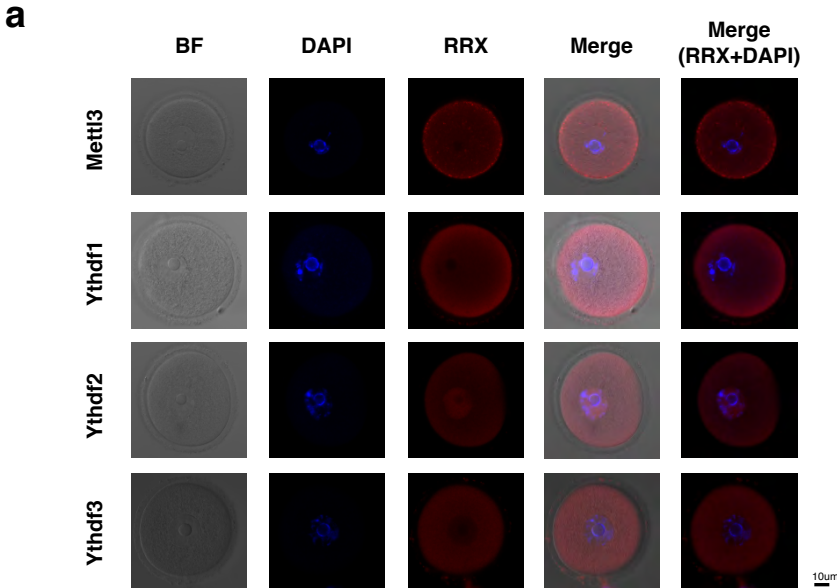
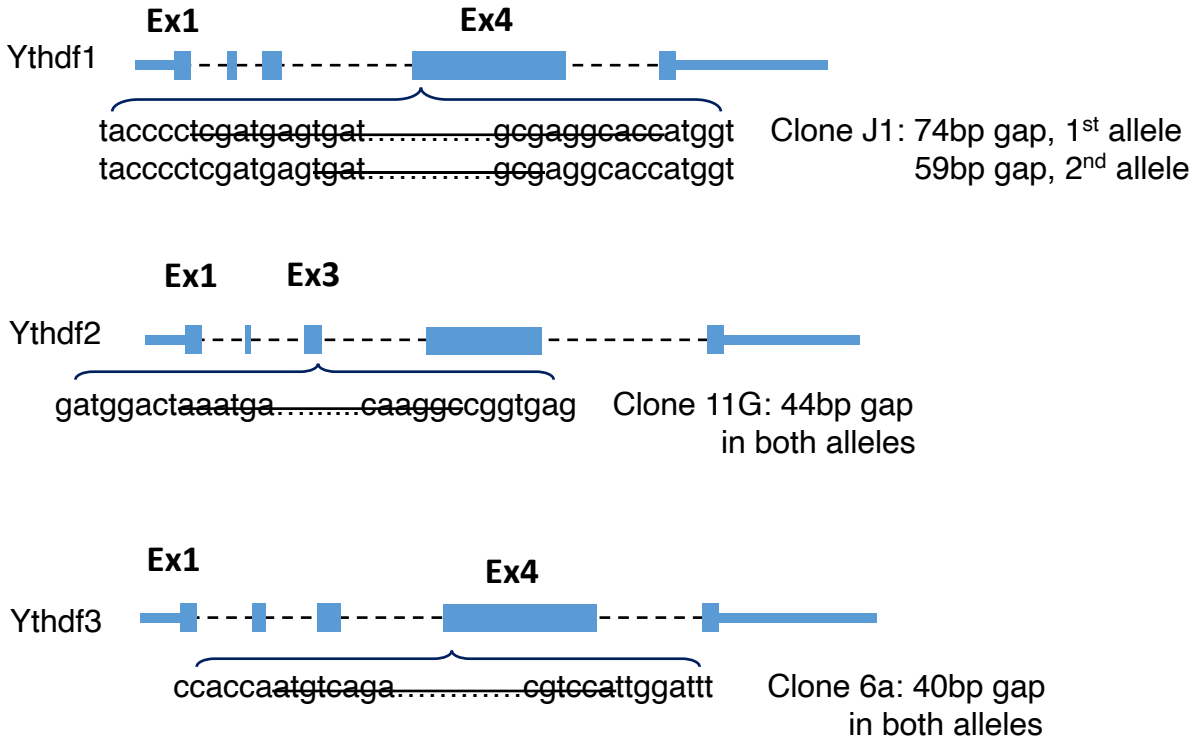


Figure S8. Generation and validation of Knock-Out mESC lines

a

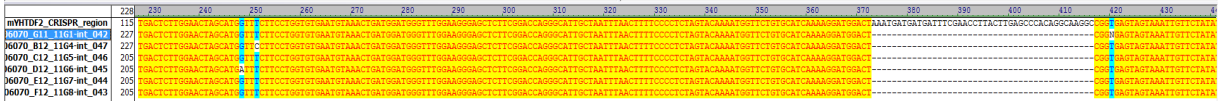


b

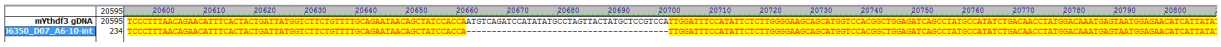
mYthdf1 Clone J1 - 74bp gap 59bp gap



mYthdf2 Clone 11G - 44bp gap



mYthdf3 Clone 6A - 40bp gap



c

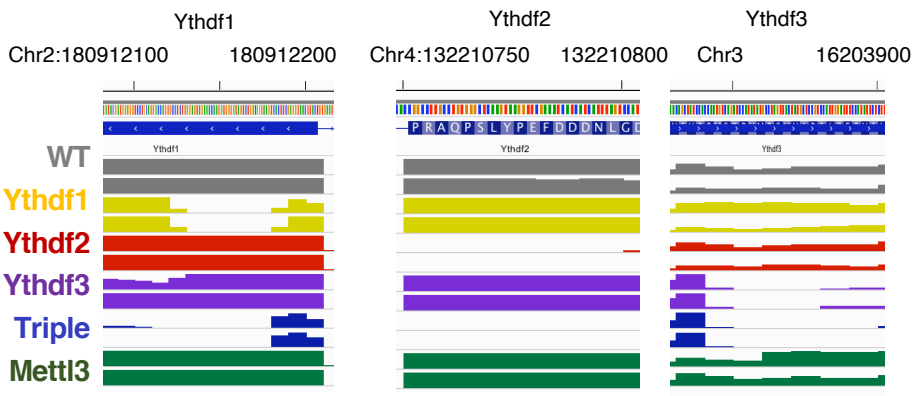
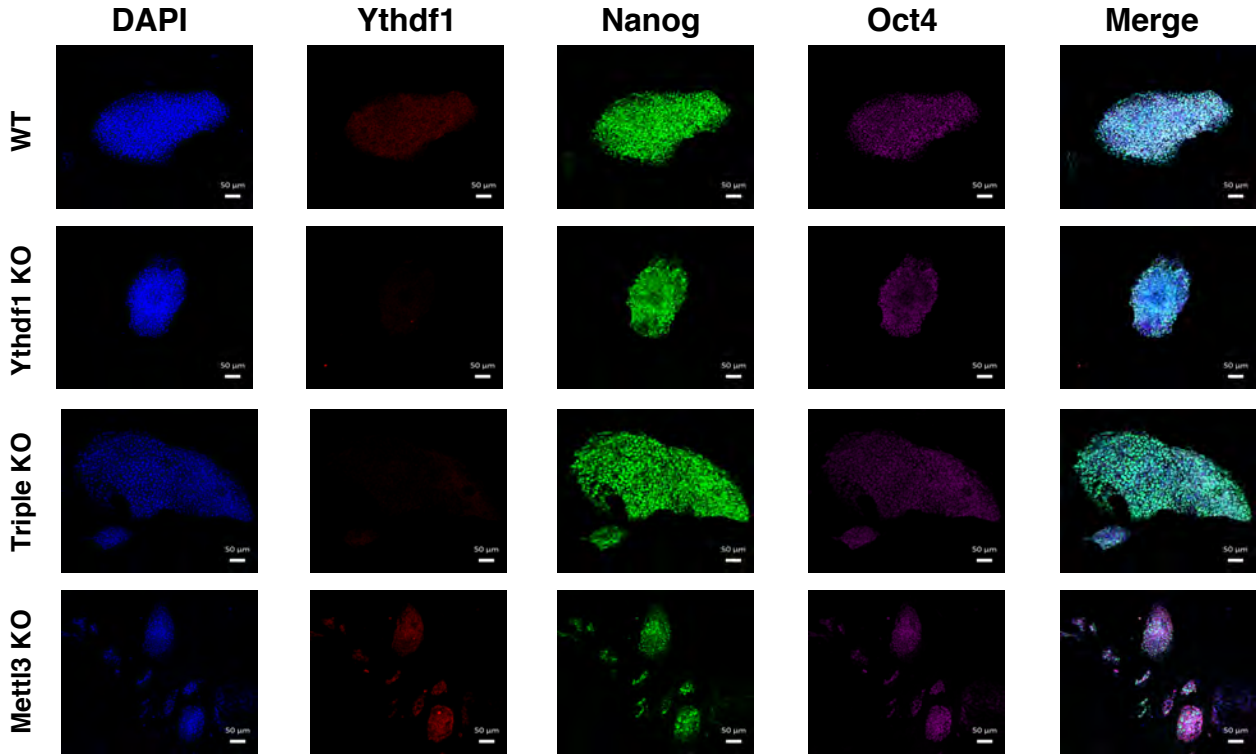


Figure S9. Generation and validation of Knock-Out mESC lines

a



b

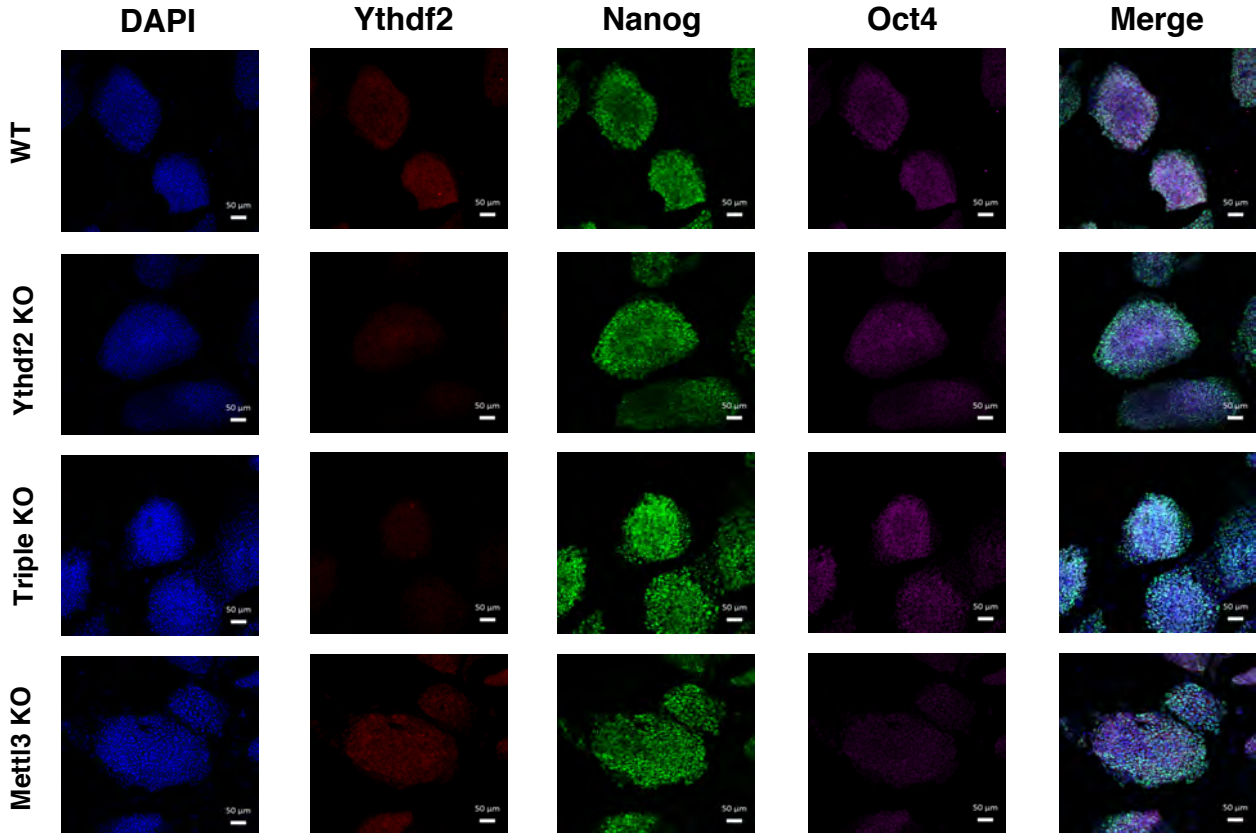


Figure S9..Cont. Generation and validation of Knock-Out mESC lines

c

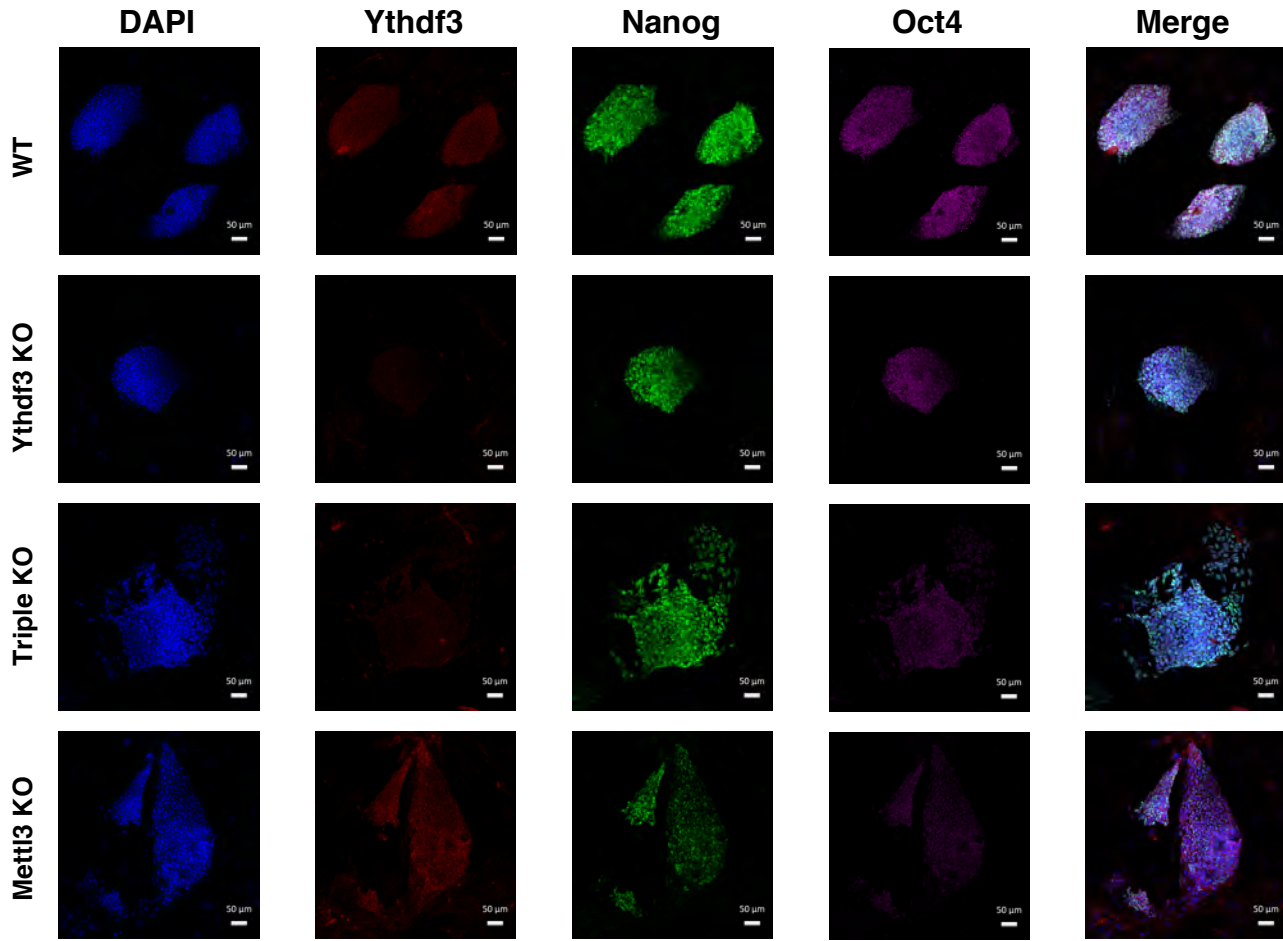


Figure S10. Morphology of Knock-Out mESC lines

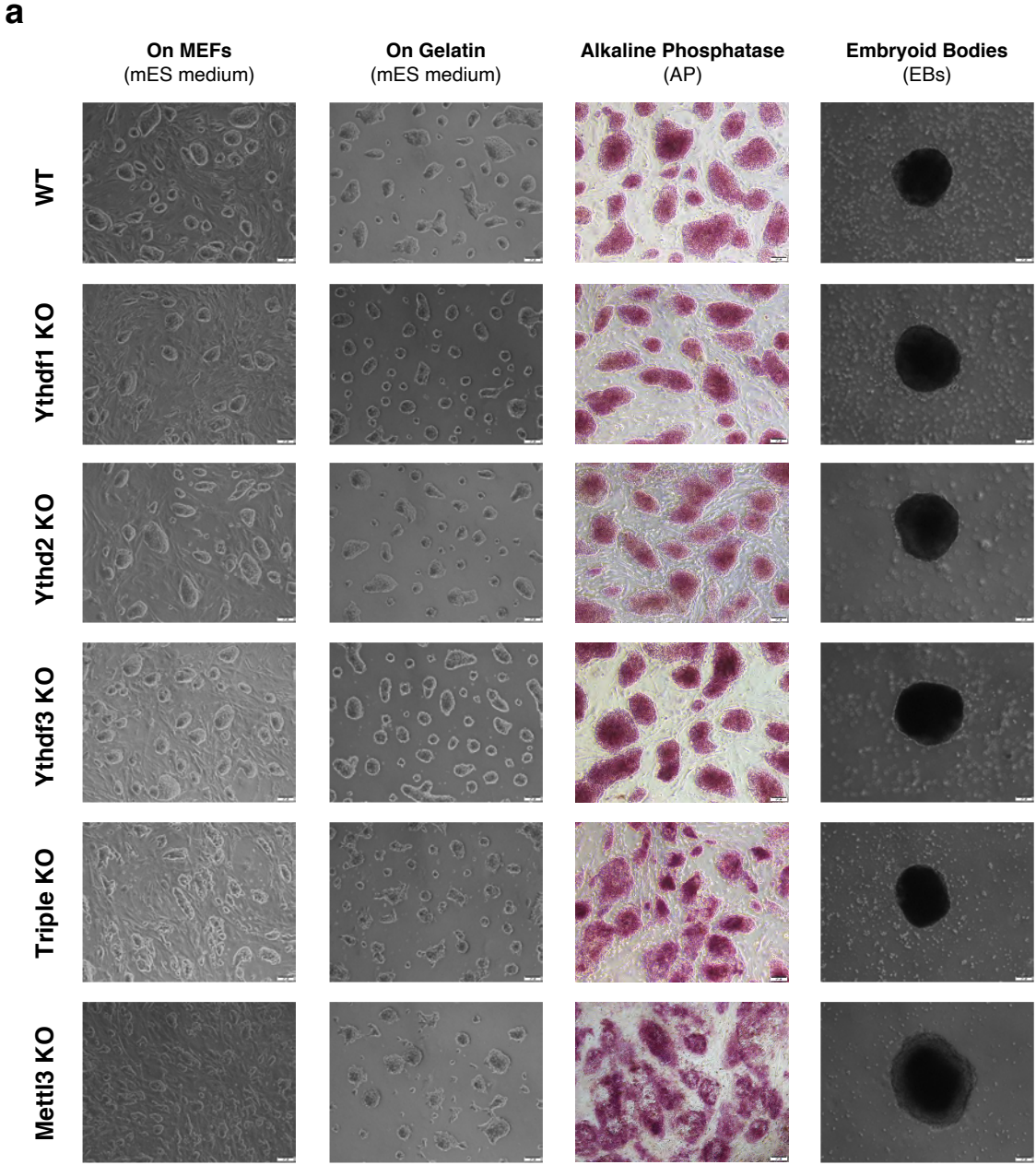


Figure S11. Overlap of ESC signatures

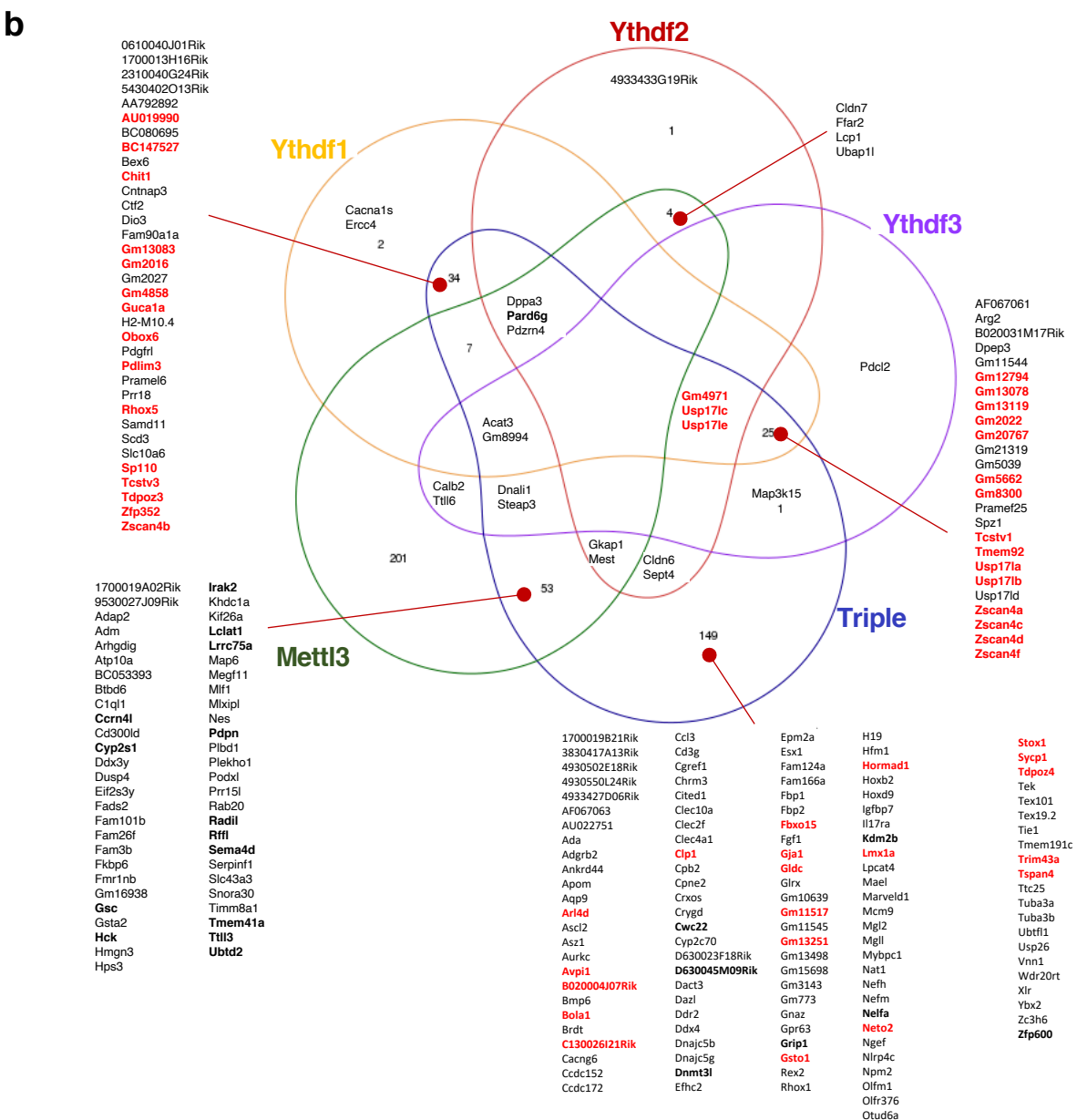
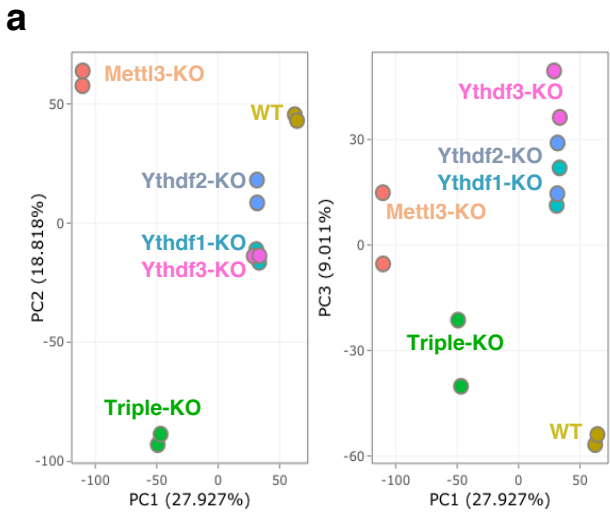
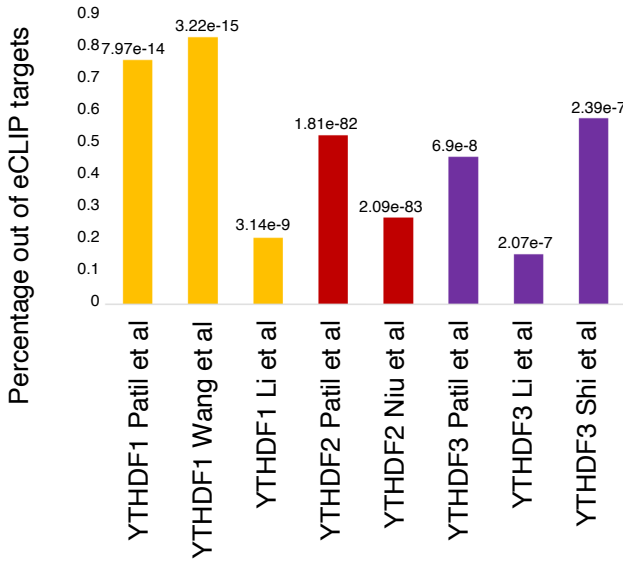


Figure S12. CLIP data evaluation

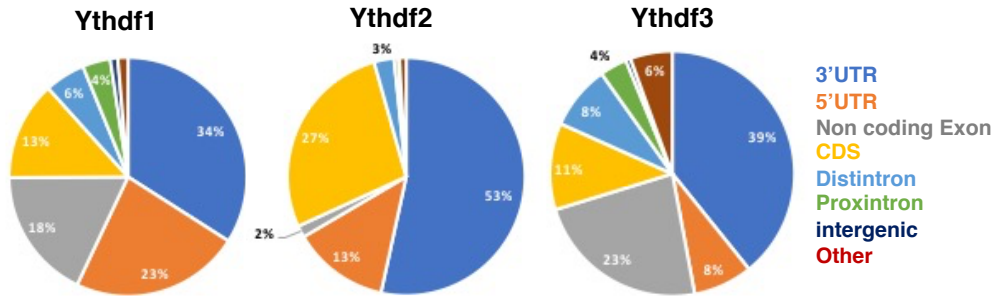
a



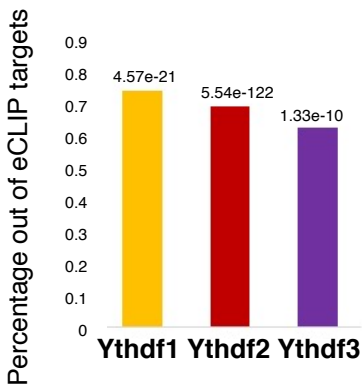
b



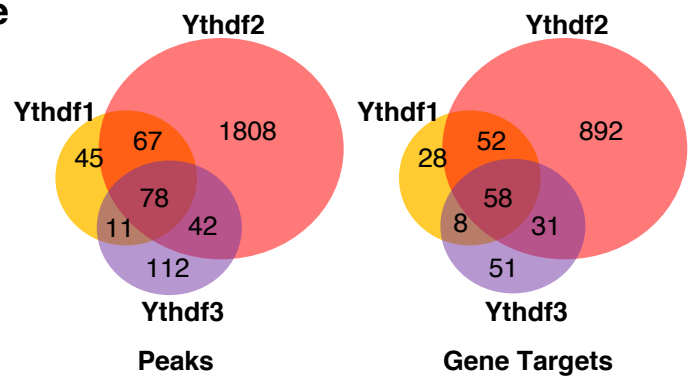
c



d



e



f

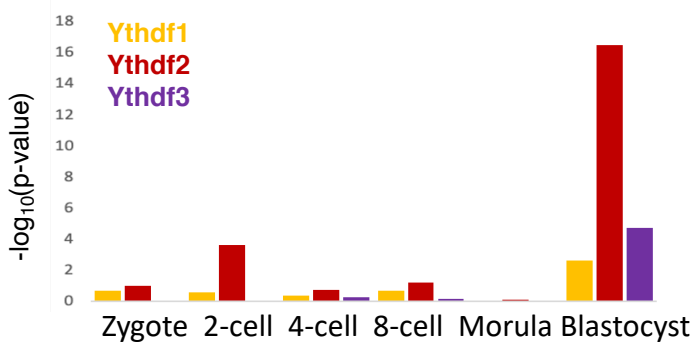
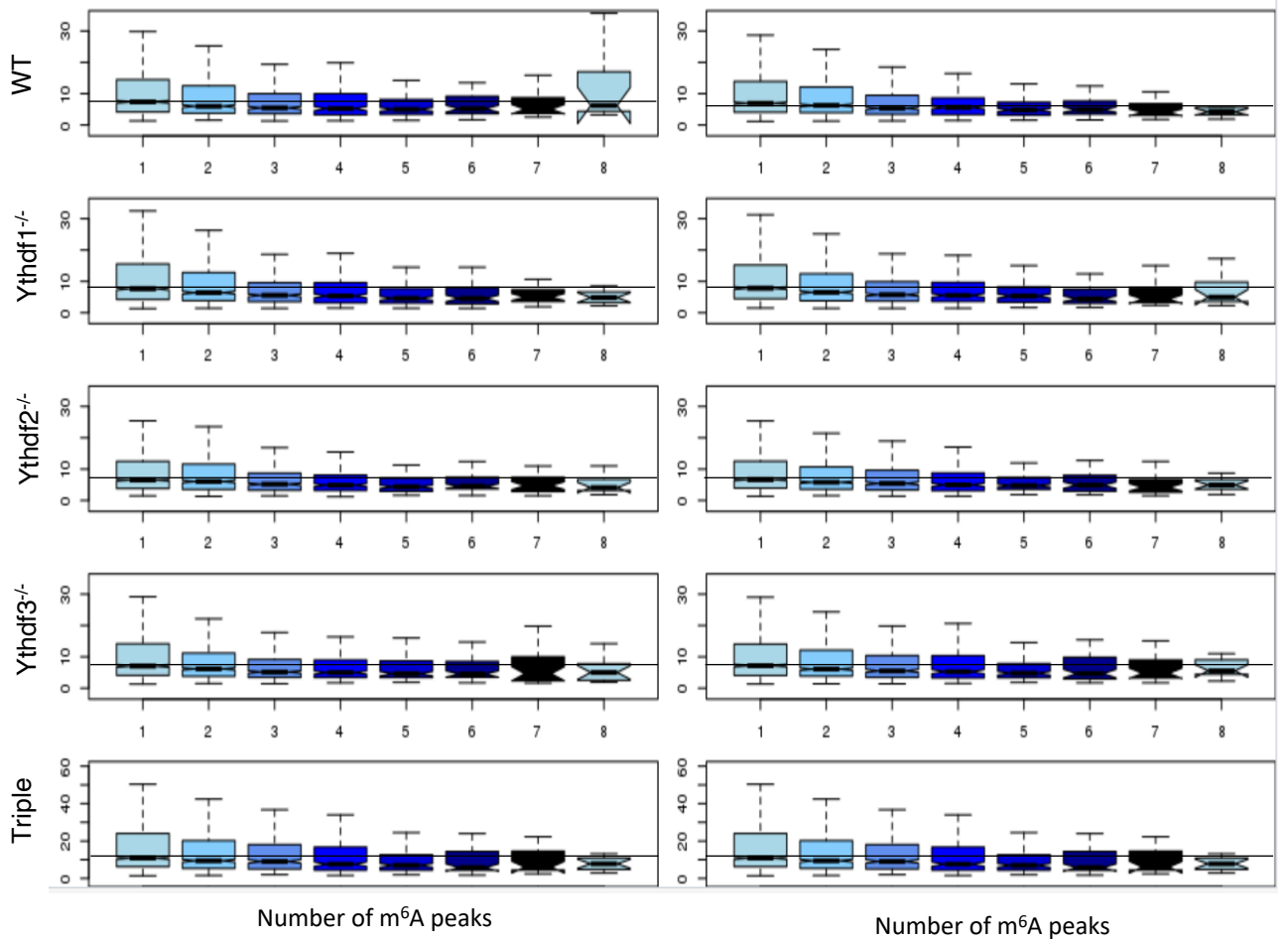


Figure S13. Half life as a function of number of m⁶A peaks

a



b

